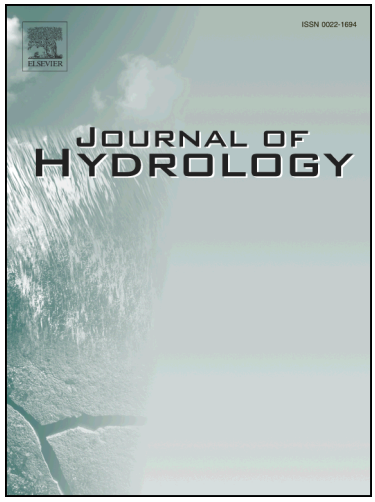

Research papers

Estimating retention potential of headwater catchment using Tritium time series

Harald Hofmann, Ian Cartwright, Uwe Morgenstern

PII: S0022-1694(18)30284-1
DOI: https://doi.org/10.1016/j.jhydrol.2018.04.030
Reference: HYDROL 22733

To appear in: *Journal of Hydrology*

Please cite this article as: Hofmann, H., Cartwright, I., Morgenstern, U., Estimating retention potential of headwater catchment using Tritium time series, *Journal of Hydrology* (2018), doi: https://doi.org/10.1016/j.jhydrol.2018.04.030

Estimating retention potential of headwater catchment using Tritium time series

Harald Hofmann[a,b,*], Ian Cartwright[b], Uwe Morgenstern[c]

[a]*School of Earth and Environmental Sciences, The University of Queensland, St Lucia, Queensland 4072, Australia*
[b]*School of Earth, Atmosphere and Environment, Monash University, Clayton, Victoria 3800, Australia*
[c]*Isotope Hydrology & Water Dating Lab, GNS Science, Lower Hutt 5040, New Zealand*

Abstract

Headwater catchments provide substantial streamflow to rivers even during long periods of drought. Documenting the mean transit times (MTT) of stream water in headwater catchments and therefore the retention capacities of these catchments is crucial for water management. This study uses time series of ^{3}H activities in combination with major ion concentrations, stable isotope ratios and radon activities (^{222}Rn) in the Lyrebird Creek catchment in Victoria, Australia to provide a unique insight into the mean transit time distributions and flow systems of this small temperate headwater catchment. At all streamflows, the stream has ^{3}H activities ($<$2.4 TU) that are significantly below those of rainfall ($\sim$ 3.2 TU), implying that most of the water in the stream is derived from stores with long transit times. If the water in the catchment can be represented by a single store with a continuum of ages, mean transit times of the stream water range from $\sim$6 up to 40 years, which indicates the large retention potential for this catchment. Alternatively, variations of ^{3}H activities, stable isotopes and major ions can be explained by mixing between of young recent recharge and older water stored in the catchment. While surface runoff is negligible, the variation in stable isotope ratios, major ion concentrations and radon activities during most of the year is minimal ($\pm$ 12%) and only occurs during major storm events. This suggests that different subsurface water stores are activated during the storm events and that these cease to provide water to the stream within a few days or weeks after storm events. The stores comprise micro and macropore flow in the soils and saprolite as well as the boundary between the saprolite and the fractured bed rock. Hydrograph separations from three major storm events using Tritium, electrical conductivity and selected major ions as well a δ^{18}O suggest a minimum of 50% baseflow at most flow conditions.

We demonstrate that headwater catchments can have a significant storage capacity and that the relationship between long-water stores and fast storm event subsurface flow is complex. The study also illustrates that using ^{3}H to determine mean transit times is probably only valid for baseflow conditions where the catchment can be represented as a single store.

The results of this study reinforce the need to protect headwater catchments from contamination

*h.hofmann@uq.edu.au

and extreme land use changes.

Keywords: Mean transit times, Tritium Time Series, Headwater catchment, Hydrograph Separation

1. Introduction

Documenting the time taken for water to flow through a catchment until it discharges into the stream network (the transit time) is crucial for understanding catchment hydrological responses and for water resource protection and management (Kirchner et al., 2010; McDonnell et al., 2010; Morgenstern et al., 2010; Hrachowitz et al., 2013). Water management authorities have mostly focussed on lowland rivers and larger catchments where rivers flow through low-gradient, well-developed alluvial valleys, while neglecting the storage capacities of headwater catchments. However, headwater streams typically comprise over two-thirds of total stream length and contribute a significant proportion of the total flow of many river systems, especially at low-flow conditions (Freeman et al., 2007). This in turn means that the headwater catchments provide much of the water supply for communities, agriculture, and industry further downstream.

Groundwater from the near-river alluvial sediments generally contributes water to perennial lowland rivers during low-flow periods (baseflow conditions) (Sophocleous, 2002; McCallum et al., 2010; Cook, 2013). By contrast, headwater catchments are commonly developed on indurated or crystalline rocks and lack extensive alluvial groundwater systems. The observation that many streams in headwater catchments continue to flow over prolonged dry periods indicates that there are stores of water (in soils, weathered basement rocks, or fractures) with retention times of at least a few years (Maloszewski et al., 1983, 1992; Rice and Hornberger, 1998).

Protecting headwater catchments is vital. While many upper catchments retain native vegetation and are protected under national park legislation, increasing population growth as well as economic development have led to progressive changes in landuse in these areas, including plantation forestry, agriculture, and peri urban developments. The impacts of such development on the catchments, and consequently on the river systems as a whole, is currently poorly understood. Understanding the timescales of water movement within the catchments and the importance of the different water stores is essential for understanding flow generation and providing catchment characteristic baselines for water management authorities.

1.1. Runoff processes in headwater catchments

That headwater catchments provide substantial flow to river systems even during prolonged dry periods implies that they store and eventually release water back into the rivers (Becker, 2005). Many

geochemical studies suggest that a large component of storm runoff is also composed of water that has been stored in the catchment rather than direct surface runoff; this is often termed the 'old water paradox' (Sklash and Farvolden, 1979; Kirchner, 2003; McDonnell et al., 1990; Kienzler and Naef, 2008). There are two main mechanisms by which 'old' water emerges in streams, firstly displacement of stored water by infiltrating rainfall and secondly a pressure wave propagation from the infiltrating rain resulting in increased groundwater discharge to the stream (hydraulic loading) (Klaus et al., 2013). The total groundwater or subsurface flow is a sum of water release from all subsurface stores, including deeper groundwater, soil water and interflow. There has been significant research into distinguishing faster from slower subsurface flow (Jencso and McGlynn, 2011; Bogaart et al., 2013; Berne et al., 2005). Several studies have shown that flow at the hillslope scale is a combination of matrix flow or displacement mixed with preferential flow. The ratios of matrix flow to preferential flow vary widely between studies and catchments and range from 1 to 90 % (Leaney et al., 1993; Kumar et al., 1997; Vogel et al., 2010; Allaire et al., 2009; Stumpp and Maloszewski, 2010). The variability of the distribution of matrix flow versus preferential flow is linked to soil types, geology and vegetation (Klaus et al., 2015). Preferential flow paths such as macropores (soil pipes), cracks from clay shrinkage, root channels and animal burrows provide path ways with a multitude of flow velocities, which are generally well above those of water travelling through the soil matrix pores (Davies et al., 2013; Kienzler and Naef, 2008; Beven and Germann, 2013; van Schaik et al., 2014). The dynamic mixing and displacement of groundwater with these ranges of velocities create a complexity in catchment response and therefore also influence the transit times. The mean transit time at a catchment outlet then represents a mix of water from all different flow paths.

1.2. Determining transit times in headwater catchments

There are several methods that may be used to determine the transit times of water in catchments (McDonnell et al., 2010). As transit times increase, any variation in the geochemistry of rainfall is progressively attenuated. Thus, comparing the temporal variation of stable isotope ratios or major ion concentrations in the stream water with those in rainfall can be used to derive transit times (McGuire and McDonnell, 2006; McDonnell et al., 2010; Kirchner et al., 2010; Hrachowitz et al., 2013). Mean transit times of stream water have also been estimated by fitting the variability of stable isotope ratios in the stream water to those of rainfall with sine wave functions (Rodgers et al., 2005; Tetzlaff et al., 2007; Tekleab et al., 2014). Alternatively, when combined with models that describe the distribution of flow paths in a catchment (Maloszewski, 2000), the variation in stable isotopes or major ion geochemistry at the catchment outlet can be used to quantify mean transit times. While this approach has been applied with some success, there are several limitations. Firstly, it requires high-frequency

(ideally sub-weekly) stable isotope and/or major ion geochemistry rainfall and streamflow records of at least the duration of the transit time of water in the catchment (Timbe et al., 2015); these records are not commonly available especially where transit times are more than a few years. Secondly, a single estimate of the transit time is commonly made, whereas water of different ages may contribute to the stream at baseflow and higher flow conditions (Morgenstern et al., 2010; Morgenstern and Daughney, 2012). Finally, the above mentioned tracers are ineffective where transit times are in excess of 4-5 years as the initial tracer variation over time is attenuated (Stewart et al., 2010; Duvert et al., 2016).

Tritium (^{3}H) is an ideal tracer for determining water transit times in catchments. ^{3}H is part of the water molecule and its abundance in water isolated from the atmosphere is controlled only by radioactive decay and not by reactions between the water and the aquifer matrix (as is the case with some solute tracers). It has a half-life of 12.32 years, and with high-precision low-background analyses (Morgenstern and Taylor, 2009), it can be utilised to estimate mean transit times of over 100 years (Morgenstern et al., 2010). The ^{3}H input function in rainfall has a distinct peak in the 1950s to 1960s due to the production of ^{3}H by the atmospheric thermonuclear tests (the so-called 'bomb pulse'). Traditionally, the propagation of the bomb pulse has been utilised to trace the flow of water recharged during this period (Fritz et al., 1991; Clark and Fritz, 1997). Since the mid 1960s atmospheric ^{3}H activities have declined. In the northern hemisphere, single ^{3}H measurements currently yield non-unique mean transit time estimates (although mean transit times may be estimated using ^{3}H time series). The bomb pulse ^{3}H peak was several orders of magnitude lower in the southern hemisphere than in the northern hemisphere (Clark and Fritz, 1997; Morgenstern et al., 2010), and the ^{3}H activities of remnant bomb pulse water have now decayed well below those of modern rainfall. This allows unique mean transit times to be estimated from single ^{3}H activities (Morgenstern et al., 2010; Morgenstern and Daughney, 2012). Consequently, the transit time of stream water can be determined for a specific time or at different streamflows. By extension, ^{3}H can be used to test whether older and younger reservoirs contribute water to streamflow at different stages of the hydrological cycle. Because ^{3}H activities in rainfall have been measured globally for several decades (Global Network or Isotopes in Precipiation, 2016; Tadros et al., 2014), ^{3}H input into many catchments is relatively well known. Calculating precise transit times may be difficult due to the unknown complexity of the catchment flow system. However, since the ^{3}H bomb pulse has mostly disappeared in the southern hemisphere, relative transit times do not depend on the accuracy of the assumed flow model and water with low ^{3}H activities has longer transit times than water with tritium activities closer to those of rainfall. This in turns, allows tritium activities to be directly compared to other parameters, such as streamflow, stable isotopes and major ion concentrations (Cartwright and Morgenstern, 2015).

1.3. Understanding water sources

Soil water, runoff, and groundwater from aquifers with different mineralogy most likely have different major ion and trace element geochemistries (Gaillardet et al., 1999; Herczeg and Edmunds, 2000; Cartwright et al., 2007, 2012; Cartwright and Morgenstern, 2012; Soulsby and Tetzlaff, 2008; Hofmann and Cartwright, 2013; Edmunds, 2009). For example, soil water commonly has elevated Si and K concentrations, waters derived from sedimentary rocks may have higher Ca concentrations if carbonate dissolution has occurred, and waters from granitic aquifers commonly have high Na, K or Ca concentrations due to the weathering of feldspar and other silicate minerals (Hofmann and Cartwright, 2013).

The stable isotope ratios of water leaving a catchment progress towards the weighted mean value of annual rainfall when residence times in the catchment are sufficient to attenuate seasonal variations. Although this precludes their use in terms of transit time estimations, they can be used to separate the baseflow during high flow periods via a mass balance (Hugenschmidt et al., 2014).

Radon (^{222}Rn), which is part of the ^{238}U to ^{206}Pb decay series, is commonly used to determine the distribution and quantity of groundwater inflows to streams and rivers (Cartwright et al., 2014b; Cook, 2013). ^{222}Rn reaches secular equilibrium with its parent isotope ^{226}Ra over a few weeks (Cecil and Green, 2000). The concentration of ^{226}Ra in minerals is several orders of magnitude higher than dissolved ^{226}Ra in surface water, which results in ^{222}Rn activities in groundwater also being orders of magnitude higher than in streams (Cook, 2013; Cecil and Green, 2000). Adsorption of ^{226}Ra onto hydroxides, clays and organic substrates may increase ^{222}Rn activities in soils and weathered rocks (Chabaux et al., 2011). High ^{222}Rn activities in surface water therefore indicate that groundwater or soil water discharges into the stream. The differentiation between groundwater and soil water or interflow using ^{222}Rn is difficult. ^{222}Rn activities in the soil waters are commonly higher than in water from the saprolite or the bedrock due to the higher emanation potential in the weathered soils. While ^{222}Rn requires approximately three weeks to reach secular equilibrium dissolution of already existing ^{222}Rn in the unsaturated zone occurs instantly when rain water infiltrates into the subsurface and mixes with the existing soil air (Surbeck, 1993).

1.4. Aims and objectives

The aim of the project was to investigate headwater mean transit times in a small (7.3 km^2) temperate headwater catchments in Victoria, Australia at varying streamflows. The project integrates monthly tritium activities, major ion concentrations, stable isotopes ratios and ^{222}Rn activities collected over a years. The tritium and stable isotope data are used to estimate the transit times of water in the catchment. The catchment behaviour is investigated by high frequency sampling over storm

events. The combination of stable isotope, major ion chemistry and ^{3}H data over storm events is used to assess the changing stores of water in the catchment. Despite the advantages of ^{3}H in directly understanding the transit times of water during high streamflow, it has been little used for this purpose (Crouzet et al., 1970; Kennedy et al., 1986). With the diminishing of the bomb pulse, ^{3}H holds the potential to resolve the inputs from different water stores during high streamflows and thus allows to better understand how catchments respond to rainfall.

2. Methods

2.1. Site description and catchment characteristics

The Lyrebird Creek catchment is part of the Yarra River catchment and is located in the Dandenong Ranges National Park west of Melbourne, Australia (Fig. 1). It is a 7.3 km^2 headwater catchment, and is mostly covered ($\sim$90 %) in pristine eucalypt forest with dense undergrowth vegetation. Lyrebird Creek is a first-order stream draining the catchment to the northeast. The southern catchment boundary is the highest part of the catchment with an elevation of $\sim$580 m, while the catchment outlet at Olinda Road is at 220 m (Fig. 1). Average yearly rainfall at Montrose (approximately 5 km west of Lyrebird Creek) between 2009 and 2014 is $\sim$1044 mm (Australian Bureau of Meteorology, 2015) with an average evapotranspiration loss over the same period of $\sim$75 %. In this temperate climate, most of the rainfall occurs during the austral winter while the highest evapotranspiration rates occur during summer. Average summer temperatures range from $\sim$11-30°C and winter temperatures range from 3.5-13°C (Australian Bureau of Meteorology, 2015).

Lyrebird Creek is perennial at the catchment outlet at Olinda Road; however, the reaches upstream of Boundary Road (Fig. 1) may dry up in summer. Flow at Olinda Road between 2006 and 2013 ranged from 0.48 to 52.9 ML day^{-1}. The flow varies with annual rainfall, with a median flow (Q50) of $\sim$3.91 ML day^{-1} for the period from 2000 to 2012 (Samantha Imberger, University of Melbourne, personal communications). Due to the below average rainfall, the median flow was 2.1 ML day^{-1} in 2013 (Fig. 2). The gentle slope of the flow duration curve and a 90 % occurrence of flows smaller than 8.43 and 4.64 ML day^{-1} indicates that surface runoff only occurs after major storm events. The average annual flow of Lyrebird Creek is $\sim$1550 ML but the 2013 flow was 67 % of the long-term average at $\sim$1140 ML. This is due to rainfall in 2013 being lower (982.6 mm) than the average of 1044 mm (Australian Bureau of Meteorology, 2015). Streamflows were low ($\sim$1.34 ML day^{-1}) during April 2013 and May 2013 as a consequence of a relatively dry summer. Monthly flows increased to peaks of 34.08 ML day^{-1} in November 2013 after intensive rainfall with monthly rainfall totals of over 100 mm for August, September and October and November.

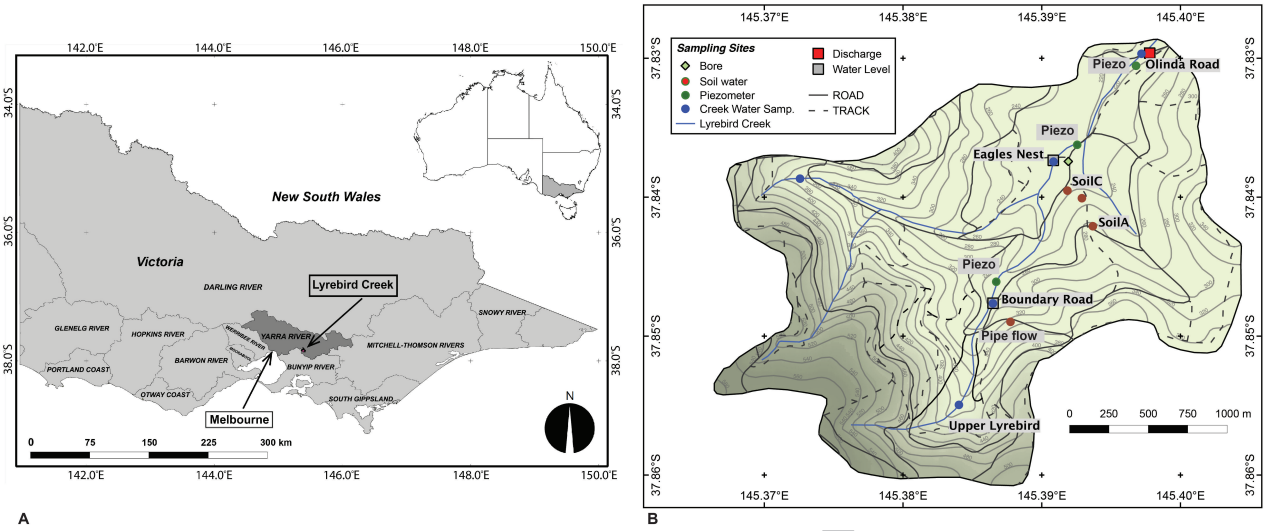

Figure 1: A) Overview map of the location of the catchment in Victoria, Australia. B) Map of the Lyrebird Creek catchment and the sampling sites. Soil sample locations represent suction-cup samplers and 'Piezo' represents the locations of piezometers in the creek banks, approximately 1-2 m away from the creek. Explanation of the legend: *Bore* = Deep groundwater bore in the fractured rock aquifer, *Soil water* = Soil sampling suction cups, *Piezometer* = shallow groundwater piezometers, *Creek Water Samp.* = Lyrebird Creek water sampling points, *Water level* = Position of water level loggers, *Discharge* = Locations where water level is converted to discharge with rating curve.

The Lyrebird catchment lies within Dandenong Ranges Igneous Complex, which consists of Devonian volcanic rhyolitic and dacitic ignimbrites. Hornfels in the east of the catchment forms the boundary between the Devonian volcanics and Palaeogene tholeiitic lava flows (Tweed et al., 2005, 2006). The volcanic rocks are underlain by Palaeozoic marine metasediments of the Lachlan Fold Belt, which underlie most of the Melbourne region. There are minor deposits of Quaternary alluvium along the streams in the northern central part of the Lyrebird catchment. Deep saprolitic weathering forms kaolinite-rich, red, loamy soils. The total depth is unknown but is estimated at $\sim$1.5 m at the top of the catchment to 3 m at the catchment outlet. Hand augering showed that the root zone of the vegetation penetrates the soils to at least 2 m. The lower altitude alluvial areas are rich in clay and organic matter which results in swampy waterlogged areas in the proximity of the Lyrebird Creek that are regularly flooded. The Palaeozoic basement comprises an unconfined fractured rock aquifer. Due to the complex geology and the high degree of fracturing, groundwater flow is variable but the general flow direction follows the topography to the North towards the Yarra River. Tweed et al. (2005) investigated the larger Dandenong Ranges area and suggested that the catchment is relatively variable with respect to rainfall and recharge with bore hydrographs responding to seasonal precipitation changes with a lag of 2 to 3 months.

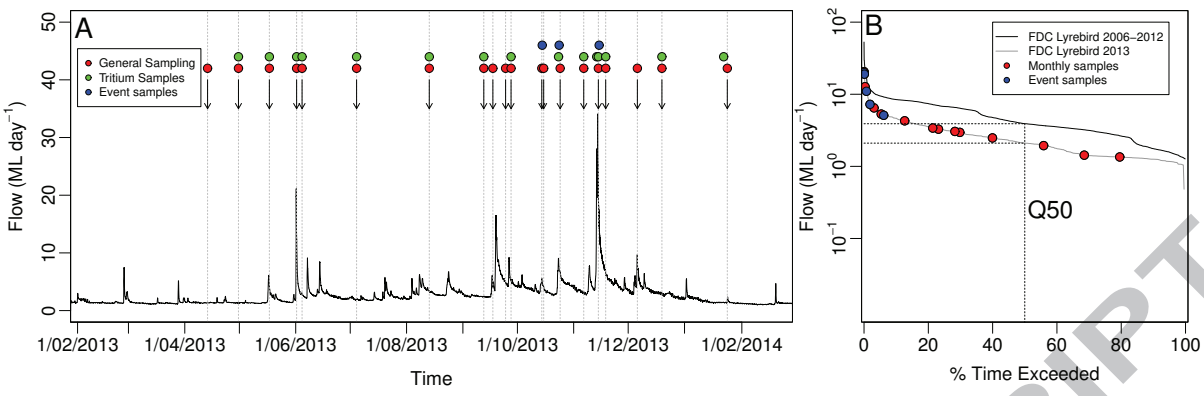

Figure 2: A) Figure shows sample times throughout 2013 and 2014 and the stream flow for the studied period. Red points indicate all the dates when general water chemistry samples were taken, green points indicate all dates for which Tritium was measured and blue points indicate the three storm events that were sampled. B) Samples in relation to the flow when samples were taken and the flow duration curve.

2.2. Sample collection

Lyrebird Creek was sampled at least monthly at the catchment outlet at Olinda Road and Boundary Road, which is the furthest upstream location where the stream is perennial, between April 2013 and February 2014 (Fig. 1). Stream water was sampled directly from the stream into 1 litre high-density polyethylene (HDPE) bottles. In addition to the monthly samples, stream water was collected at Olinda Road over three storm events, two minor events in October 2013 and a major storm event in November 2013. The storm event samples were taken using an ISCO 6712 autosampler (Teledyne ISCO, Inc.) with remote trigger and a 24 x 1 litre sample carousel. The autosampler samples were collected 1 day after the storm events, bottled in 1 litre HDPE bottles refrigerated until further processing. Push point piezometers were driven into the sediments to a depth of approximately 1 m near the stream (1 - 2 m distance) at Eagles Nest and Olinda Road (Fig. 1). A small diameter bailer was used to extract water from the push point piezometers. Soil water was sampled using suction cup soil moisture samplers (UMS Germany) at depths of 40 and 80 cm at three locations; hilltop, mid-slope and valley (Fig. 1). Four water samples were also taken directly from discrete discharge points from the soils on a road cutting at Boundary Road during the November storm event. Flow at the road cutting only occurred during major storm events and were dry during the rest of the study period. Overland flow was sampled during the November storm event by collecting running water on the hillslope into 125 ml HDPE bottles. Rainwater was sampled at Monash University (approximately 30 km from field site) on an event-basis; rainwater was also collected monthly at Olinda Road using a funnel rain collector mounted $\sim$1.5 m above ground. The rain collector sampled a mixture of rainfall and throughfall under the canopy cover and was emptied monthly. A thin paraffin film was added to

the rainwater sampler to prevent evaporation. Chemical analysis of rainwater is equivalent to those of creek and groundwater, which is described below.

2.3. Geochemical and isotope analyses

Electrical Conductivity (EC) was measured in the field using a calibrated WTW Meter and probe. Continuous EC was measured at Boundary Road and Olinda Road using a WinSitu AquaTroll 200 on a 15 minutes time step. Samples for cation analysis were filtered through 0.45 μm nitrate cellulose filters and acidified to pH <2 with 16 M HNO_3 and analysed at Monash University using a ThermoFinnigan inductively coupled plasma optical emission spectrometry (ICP-OES) or inductively coupled plasma mass spectrometry (ICP-MS). Samples for anion analysis were filtered through 0.45 μm nitrate cellulose filters and analysed using a Metrohm ion chromatograph at Monash University. The precision of anion and cation analyses based on replicates is ± 2 % and the accuracy based on analysis of certified water standards is ± 5 %. HCO_3 and dissolved CO_2 with a precision of 5-10 % were determined by titration using a Hach Field titration kit. Rainfall bicarbonate concentrations were not measured due to the small volumes and long residence time in the sample containers.

δ^{18}O and δ^{2}H values were measured at Monash University using Finnigan MAT 252 and ThermoFinnigan DeltaPlus Advantage mass spectrometers. δ^{18}O was analysed via equilibration with He-CO_2 at 32°C for 24-48 h in a ThermoFinnigan Gas Bench. δ^{2}H was measured by reaction with Cr at 850°C using an automated Finnigan MAT H/Device. δ^{18}O and δ^{2}H values were measured relative to internal standards calibrated against IAEA SMOW, GISP and SLAP. Data were normalised following the method by (Coplen, 1988) and are expressed relative to V-SMOW. Precision (1σ) based on replicate analysis is δ^{18}O = ± 0.1 ‰ and δ^{2}H = ± 1 ‰.

Samples for ^{3}H were vacuum distilled and enriched by electrolysis prior to being analysed by liquid scintillation spectrometry using Quantulus ultra-low-level counters at the Institute of Geological and Nuclear Sciences (GNS), New Zealand. Following the improvements from (Morgenstern and Taylor, 2009) the sensitivity is now further increased to a lower detection limit of 0.02 TU via tritium enrichment by a factor of 95, and reproducibility of tritium enrichment of 1 % is achieved via deuterium-calibration for every sample. The precision (1 sigma) is $\sim$1.8 % at 2 TU. ^{3}H activities are expressed in tritium units (TU) where 1TU represents a ^{3}H /^{1}H ratio of 1x10-18.

^{222}Rn activities in stream water and pipe flow were determined using a portable radon-in-air monitor (RAD-7, Durridge Co.) following methods described by (Burnett and Dulaiova, 2006). A glass flask of 0.5 L was filled and ^{222}Rn was degassed for 5 min into a closed air loop of fixed volume (calibrated by manufacturer) incorporating the RAD-7. Counting times were 1/2 h for stream water. Typical relative precision is 3 % at 10,000 Bq m^{-3} and $\sim$10 % at 100 Bq m^{-3}. Soil water samples

from suction cups were too small for ^{222}Rn analysis and the vacuum in the sample container would induce degassing. ^{222}Rn emanation rates were estimated from three soil samples collected at the top of the catchment at Boundary Road, in the middle of the catchment at Eagles Nest and at the lower catchment at Olinda Road. Dried soil samples of known weight were filled in airtight containers. Distilled water was then added and the container was closed for 5 weeks by which time the rate of ^{222}Rn production and decay have reached secular equilibrium. After 5 weeks, 40 ml of pore water was extracted and analysed for ^{222}Rn using the same method as described above but with counting times of 12 hours. Emanation rates γ and equilibrium ^{222}Rn activities of the sediments in the catchment were calculated from the ^{222}Rn activity of the extracted pore water following Lamontagne and Cook (2007), assuming a matrix density of 2800 kg m^{-3} and a porosity of 0.35, which are appropriate for silty soils with moderate clay content.

2.4. Estimating Transit Times

The time taken for water to flow through a catchment from where it recharges to where it discharges into a stream (the transit time) can be estimated using simplified lumped parameter models that reflect the geometry and distribution of flow paths within a catchment (Stewart and Fahey, 2010; Jurgens et al., 2012). These models are based on simplified aquifer geometries and account for effects of dispersion and mixing of water that has followed flow paths of different lengths (Jurgens et al., 2012). For steady-state flow, the convolution integral relates the tracer input over time (C_{inp}) and the tracer concentration at the catchment outlet (C_{out}) (Maloszewski, 2000):

$$C_{out} = \int C_{inp}(t-\tau)h(\tau)exp(-\lambda\tau)d\tau \quad (1)$$

where *t* is the sampling time, τ is the transit time, *h* (τ) is the flow model or response function of the hydrological system, and λ is the decay constant (0.0563 yr^{-1} for ^{3}H). The exponential term represents the radioactive decay of ^{3}H (Stewart et al., 2010).

Lumped parameter models are most easily applied to conservative tracers (such as ^{3}H or the stable isotopes) that migrated at the same rate as the water (Jurgens et al., 2012). The application of these models to a specific catchment requires a conceptual understanding of the geometry of the groundwater flow system. The exponential flow model (EM) describes mean transit times in a homogeneous, unconfined aquifer of constant thickness and with uniform recharge. The combined flow to a stream at the outflow constitutes water from flow paths from the entire aquifer that have an exponential transit time distribution (Stewart et al., 2010). The piston flow model (PFM) assumes linear flow with no mixing within the aquifer such that all water discharging to a stream at one point in time has the same transit time. One of the most commonly used models is the exponential piston flow model (EPM). It

is a combination of the piston flow model where the catchment has regions of linear flow and regions where the flow paths have an exponential distribution (Morgenstern et al., 2010). The solution to 1 for the exponential piston flow model is given by Zuber et al. (2005):

$$h(\tau) = 0 \qquad for \quad \tau_m(1-f) \tag{2}$$

$$h(\tau) = (f\tau_m)^{-1} \cdot exp\left[-\left(\frac{\tau}{f\tau_m}\right) + \left(\frac{1}{f}\right) - 1 \right] \qquad for \quad \tau \geq \tau_m(1-f) \tag{3}$$

where τ_m is the mean residence time and f the ratio of the volume of the aquifer that exhibits exponential flow to the total aquifer volume. The EPM is widely used to estimate transit times in catchments where the water in the stream follows flow paths of varying lengths but where parts of the aquifer are confined or where there is vertical recharge through the unsaturated zone above an aquifer that exhibits exponential flow (Stewart et al., 2010; Cartwright and Hofmann, 2016).

The dispersion model (DM) is based on the one-dimensional advection dispersion equation for fluid flow in porous media (Maloszewski, 2000; Jurgens et al., 2012). While not always considered to be a realistic conceptualisation of the flow system, it has been shown to reproduce time series of tracer activities (Stewart et al., 2010). It incorporates two parameters, a mean age and a dimensionless dispersion parameter (DP). DP is the inverse of the Peclet Number and describes the relative importance of dispersion and advection (DP= D/(v x) where D is the dispersion coefficient in m^2 day^{-1}, v is velocity in m $day^{-}1$ and x is distance in m)((Jurgens et al., 2012)).

$$h(\tau) = \frac{1}{\tau\sqrt{4\pi DP\ (\tau/\tau_m)}} exp\left[-\frac{(1-\tau/\tau_m)^2}{4DP(\tau/\tau_m)} \right] \tag{4}$$

$$DP = dispersion\ parameter = \frac{Dispersion\ coefficient\ (D)}{vx}$$

Together, these are the most commonly used lumped parameter models for determining mean transit times (McGuire and McDonnell, 2006). In catchments where long time-series (i.e. several years) data are available, they have reproduced the measured variation in ^{3}H activities over time (Maloszewski and Zuber, 1982; Zuber et al., 2005; Gusyev et al., 2013; Morgenstern et al., 2015). The mean transit times were calculated by comparing the observed ^{3}H activity with those predicted by the transit time model Jurgens et al. (2012). Because ^{3}H activities are not affected by reactions in the unsaturated zone, the estimated mean transit times reflect both recharge through the unsaturated zone and flow through the aquifers.

2.5. Mass balance calculations and binary mixing models

If sufficiently large, the difference in major ion concentration, stable isotope ratios, ^{3}H or ^{222}Rn activities in subsurface water and rainwater can be used to estimate the contributions of baseflow and storm event water (Sklash and Farvolden, 1979; Godsey et al., 2009) via:

$$Q_{out}C_{out} = Q_{event}C_{event} + Q_{base}C_{base} \quad (5)$$

C_{out} and Q_{out} are the flow and tracer concentration at the catchment outlet, Q_{event} and C_{event} are the flow generated by surface runoff and interflow and tracer concentrations of rainfall and Q_{base} and C_{base} are the flow and tracer concentration of subsurface catchment water stores.

3. Results

The presentation of the results is split in two parts: first the monthly sampling that constrains general catchment behaviour, and second the short-term storm event sampling that encapsulates catchment behaviour following storm events. The distinction is made on the frequency occurrence of flows where 0 to 10 % (Q10) represents high flows and >10 % represents low flows (Fig. 2). The equivalent flow value for Q10 is $\sim$ 5ML/day. The results from monthly observations are discussed first.

3.1. Tritium activities

An accumulated rainwater sample collected at Monash University between May and December 2013 had a ^{3}H activity of 2.72 TU. A 12 months rainfall sample from Yarra Junction ($\sim$30 km NW of the study area) collected in 2016 had a similar ^{3}H activity of 2.76 TU (Cartwright, unpublished data). The highest ^{3}H activity measured in Lyrebird Creek stream water at Olinda Road was 2.4 TU while water from the interflow through macro pores had a ^{3}H activities of 2.9 TU (Tab. 1).

The ^{3}H activities of the 13 monthly stream samples from Olinda Road and the 5 samples at Boundary Road ranged from 1.43 to 2.38 TU and 1.69 and 2.23 TU, respectively (Tab. 1). ^{3}H activities in the stream water were correlated with streamflow (r^2 = 0.91) but were always lower than those of rainfall (Fig. 3B). The lowest ^{3}H activity (1.43 TU) was recorded in April 2013 at the end of the austral summer when flow at Olinda Rd was 1.31 ML day^{-1} (Fig. 3A). The activities increased slightly to 1.84 TU after a few storm events at the end of May and the beginning of June. ^{3}H activities decreased to below $\sim$1.6 TU at multiple times during the sampling year. Highest overall streamflows in the winter and spring were 20-25 ML day^{-1}, and ^{3}H activities at these times were as high as 2.4 TU. The ^{3}H activities at Boundary Road were approximately 6.3 to 10.2 % higher than at Olinda Road but displayed a similar relationship to streamflow (Fig. 3 B).

Table 1: ^{3}H concentrations from samples taken at Olinda Road, Boundary Road and the soil discharge from road cutting at Boundary Road as well as calculated mean transit times using a piston flow model (PFM), exponential model (EMM), exponential piston flow model (EPM f=0.85) and dispersion model (DM). *nm* = not measured.

Sample	**Date of Sampling**	**^{3}H** (TU)	**^{3}H error** (TU)	**PFM** (years)	**EMM** (years)	**EPM** (years)	**DM** (years)	**Flow** (ML day^{-1})
Olinda Rd.	30/04/2013	1.44	0.03	14.3	49.3	43.8	46.3	1.35
Olinda Rd.	17/05/2013	1.74	0.03	12.3	33.3	20.3	30.5	4.28
Olinda Rd.	1/06/2013	1.84	0.04	11.5	29.3	17.3	26.8	12.73
Olinda Rd.	4/06/2013	1.58	0.03	13.0	41.0	32.8	38.0	3.06
Boundary Rd.	4/06/2013	1.76	0.04	12.3	32.5	19.5	29.5	nm
Olinda Rd.	4/07/2013	1.47	0.03	13.8	46.8	41.3	43.5	1.94
Olinda Rd.	13/08/2013	1.73	0.03	12.5	33.5	20.5	30.5	3.40
Boundary Rd.	12/09/2013	1.74	0.04	12.5	32.8	19.8	29.5	nm
Olinda Rd.	12/09/2013	1.63	0.03	12.8	37.8	30.3	34.8	2.49
Olinda Rd.	27/09/2013	1.92	0.04	11.5	25.3	15.3	22.8	5.31
Olinda Rd.	23/10/2013	2.14	0.43	10.8	17.0	12.0	15.8	8.28
Boundary Rd.	6/11/2013	1.70	0.03	12.8	34.0	21.0	31.0	nm
Olinda Rd.	6/11/2013	1.56	0.04	13.3	41.0	32.5	37.8	3.28
Olinda Rd.	13/11/2013	2.41	0.04	4.8	9.3	7.8	8.8	19.58
Boundary Rd.	14/11/2013	2.32	0.04	9.8	11.3	9.0	10.8	nm
Olinda Rd.	14/11/2013	2.38	0.04	9.5	9.8	8.3	9.5	22.14
Olinda Rd.	18/11/2013	1.80	0.04	12.0	29.5	17.5	26.8	6.83
Boundary Rd. soil	18/11/2013	2.90	0.05	1.8	2.0	0.8	2.0	nm
Olinda Rd.	19/12/2013	1.63	0.03	13.0	37.0	25.0	34.0	2.96
Boundary Rd.	22/01/2014	1.69	0.03	13.0	34.0	21.0	31.0	nm
Olinda Rd.	22/01/2014	1.56	0.03	13.3	40.5	32.3	37.3	1.44

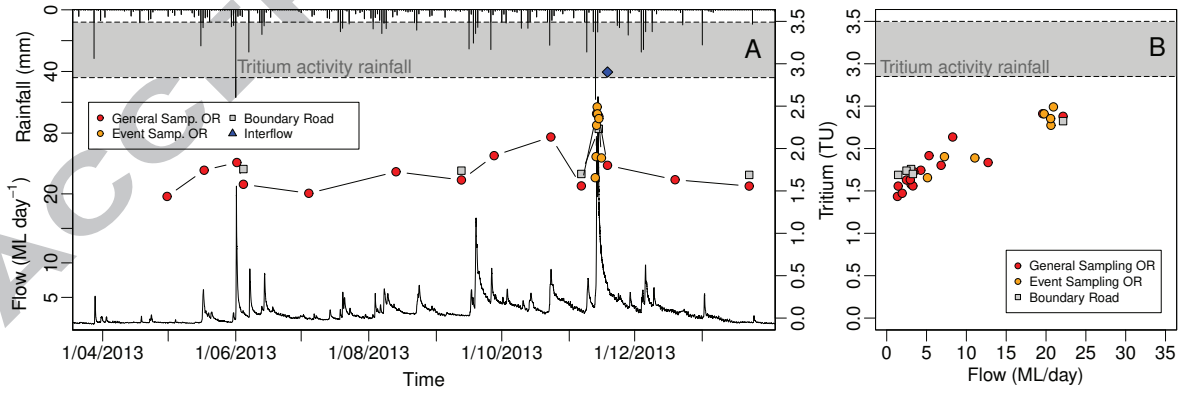

Figure 3: ^{3}H activities and streamflow in Lyrebird Creek catchment (bottom of the figure A) and rainfall (top of figure A) at Olinda Road (OR). The grey shade represents the ^{3}H rainfall variability for the area. A) ^{3}H activities over the sampled period between April 2013 and February 2014. B) Variation in ^{3}H activities with streamflow.

3.2. Stable isotopes

The δ^{18}O and δ^{2}H values of stream water from Lyrebird Creek from all sampling rounds were close to the local meteoric water line for Melbourne ((Global Network or Isotopes in Precipiation, 2016)), which has a slope of 7.48 and a D-excess of 8.75 (Fig. 4). The δ^{18}O and δ^{2}H values of the rainfall from the Lyrebird catchment had a slope of ∼6.02. δ^{18}O values were between -6.8 ‰ and -1.1 ‰ (a range of 5.7 ‰) and the and δ^{2}H values were between -44 ‰ and +6 ‰ (a range of 50 ‰). Rainfall from Melbourne (Monash University) had a much larger range (12.2 ‰ for δ^{18}O and 79.9 ‰ for δ^{2}H). Some of the difference can be attributed to the samples for Melbourne being collected on an event basis while those for Lyrebird Creek catchment were composite samples.

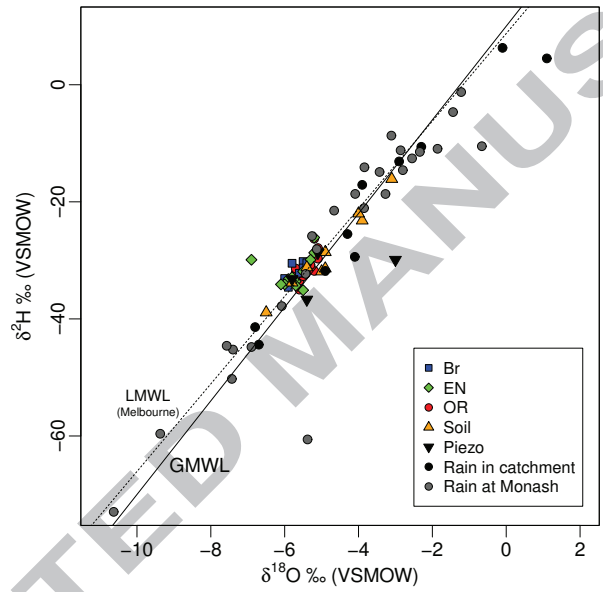

Figure 4: δ^{2}H versus δ^{18}O for the Lyrebird catchment stream water, soil water and rainfall. Grey points represent rainfall δ^{2}H and δ^{18}O for rain collected at Monash University ∼ 30 km away from the catchment. Abbreviations from the legend are: Br = Boundary Road, EN = Eagles Nest, OR = Olinda Road, Soil = Soil suction cups, Piezo = Piezometers in stream bank

The δ^{18}O and δ^{2}H values of stream water for Lyrebird Creek at Olinda Road over the sample period varied between -6.0 ‰ and -5.1 ‰ and -35 ‰ and -26 ‰, respectively (Fig. 4). The average δ^{18}O and δ^{2}H values in the stream water were similar to those of rainfall; however, the ranges are much less in the stream water. The δ^{18}O and δ^{2}H values at Boundary Road higher in the catchment were more variable, ranging between -6.5 ‰ and -3.1 ‰ and -39 ‰ and -16 ‰, respectively. The stable isotope values of the soil water samples had a similar spatial variability as the stream water stable isotope ratios. The δ^{18}O and δ^{2}H values of the soil waters ranged from -6.5 ‰ to -3.1 ‰ and -39 ‰ to -16 ‰ at Boundary Road and -5.8 ‰ to -3.0 ‰ and -37 ‰ to -29 ‰ at Olinda Road,

respectively.

3.3. Major ions and ^{222}Rn

The EC of rainfall ranged from 10 to 51 μS/cm and is similar to rainfall EC values in southeast Australia ((Blackburn and McLeod, 1983)). EC values of Lyrebird Creek at Olinda Road ranged from 86 to 115 μS/cm and those at Boundary Road ranged from 82 to 96 μS/cm, respectively. There is no correlation of the monthly measured EC values with streamflow.

Groundwater from the fractured rock basement is not accessible in the study area but soil water EC values in the Lyrebird catchment were lower than those of the groundwater, ranging from 56 μS/cm in the upper catchment at Boundary Road to 195 μS/cm in the lower catchment at Olinda Road. The temporal variability of EC in the soil water samples is minor.

There was a general downstream increase in EC values in Lyrebird Creek from 62 to 101 μS/cm at Boundary Road to 81 to 115 μS/cm at Olinda Road. While some of the high storm events are missing continuous EC data due to clogging of the logger by sediments, there was a general decrease of EC values with increasing streamflows following storm events. The lowest EC value of 62.2 μS/cm was recorded during a major storm event in October 2013.

The major ion chemistry of the stream water was dominated by Na, Cl, and HCO_3. Na concentrations ranged from 9 to 16.48 mg L^{-1} at Boundary Road and from 11.11 to 18.38 mg L^{-1} at Olinda Road (Fig. 5 A). K concentrations ranged from 1.14 to 2.0 mg L^{-1} at Boundary Road, 1.3 to 2.3 mg L^{-1} at Olinda Road. Ca and Mg concentrations ranged from 1.1 to 2.1 mg L^{-1} and 1.2 to 2.2 mg L^{-1} at Boundary Road and 1.2 to 2.3 mg L^{-1} and 1.5 to 2.5 mg L^{-1} at Olinda Road. Rainfall had Na concentrations of 1.9 to 13.5 mg L^{-1}, K concentrations of 1.0 to 4.1 mg L^{-1}, Ca concentrations of 1.1 to 7.4 mg L^{-1} and Mg concentrations of 0.36 to 3.2 mg L^{-1}. Soil water Na concentrations ranged from 7.3 to 13.8 mg/, K from 1.1 to 3.3 mg L^{-1}, Ca from 0.2 to 3.5 mg L^{-1} and Mg from 0.8 to 3.2 mg L^{-1}. Na, Ca and Mg concentrations were generally higher in the shallow groundwater from piezometers compared to the soil water with concentrations ranging from 16.1 to 23.3 mg L^{-1}, 3.6 to 6.9 mg L^{-1} and 2.8 to 5 mg L^{-1}, while K concentrations were lower ranging from 1.1 to 1.9 mg L^{-1}.

The major anions were Cl and HCO_3. Cl concentrations ranged from 12 to 18.6 mg L^{-1} at Boundary road and from 5.9 to 19.45 at Olinda Road. HCO_3 concentrations ranged from 4.7 to 8.4 at Boundary Road and from 3.9 to 11.3 mg L^{-1} at Olinda Road. SO_4 concentrations ranged from 1.8 to 2.9 mg L^{-1} at Boundary Road and 0.3 to 3.1 mg L^{-1} at Olinda Road. Rainfall had between 0.9 and 36.5 mg L^{-1} Cl and 0.14 to 4.5 mg L^{-1} SO_4. Cl concentrations in soil water ranged from 8 to 17 mg L^{-1} which is similar to those in the shallow groundwater ranging from 11.6 to 16.42 mg L^{-1}. HCO_3 was also only measures for a small number of samples due to the lack of sufficient sample.

Concentrations that were measured in the soil water ranged from 1.8 to 4.9 mg L^{-1}. SO_4 in the soil water ranged from 1 to 3.3 mg L^{-1} at Boundary Road and 0.1 to 6.4 at Olinda Road.

NO_3 concentrations in the stream were 0.7 to 8.9 mg L^{-1} at Boundary Road and 0.45 to 9.1 mg L^{-1} at Olinda Road. NO_3 concentrations in rainfall were generally below 1 mg L^{-1}. Upper catchment soil water NO_3 concentrations were also very low and comparable to those of rainfall, ranging from 0 to 0.15 mg L^{-1}. Soil water NO_3 concentrations were significantly higher in the lower catchment, ranging from 0.1 to 8.7 mg L^{-1} (Fig. 5 B).

Stream water ^{222}Rn activities were generally lower in the upper catchment than in the lower catchment, ranging from 213.8 Bq m^{-3} to 1 038.0 Bq m^{-3} at Boundary Road and 400.8 Bq m^{-3} to 1 611.0 Bq m^{-3} (median of 884.4 Bq m^{-3}) at Olinda Road. ^{222}Rn activities of the water samples from the discrete discharge points in the road cutting at Boundary during the major storm event in November 2013 were 1 930, 5 208 and 5 146 Bq m^{-3}. Calculated ^{222}Rn emanation rates (γ) from the soils were higher (8 947 $\pm$ 449 Bq m^{-3}day-1) for sediments at Boundary Road than those in the middle and the lower parts of the catchment (γ = 4364 $\pm$ 232 Bq m^{-3} day^{-1} at Eagles Nest and 2 513 $\pm$ 118 Bq m^{-3} day^{-1} at Olinda Road). Equilibrium ^{222}Rn are given by γ/λ (Cartwright et al., 2014b). The estimated γ values result in equilibrium ^{222}Rn activities of 49 709 $\pm$ 2 498, 242 248 $\pm$ 1 228 and 13 963 $\pm$ 659 Bq m^{-3} for the three locations.

3.4. Tritium, stable isotopes and major ion chemistry during storm events

Storm runoff was sampled during three storm events at the beginning of October 2013 (E1), late October 2013 (E2), and middle of November 2013 (E3). The three storm events had different streamflow magnitudes with maximum streamflows of 5.6 ML day^{-1} (E1), 9.06 ML day^{-1} (E2), and 34.08 ML day^{-1} (E3) recorded at Olinda Road (Fig. 6, Tab. 2). Storm events E1 and E2 lasted for approximately three days while the higher streamflows during the Event E3 had the highest flow and lasted for more than a week (Fig. 6). Event E3 has a double flow peak with streamflows of 28.04 ML day^{-1} at 14:00 on the 13th Nov and 34.08 ML day^{-1} at 03:35 on the 14th Nov.

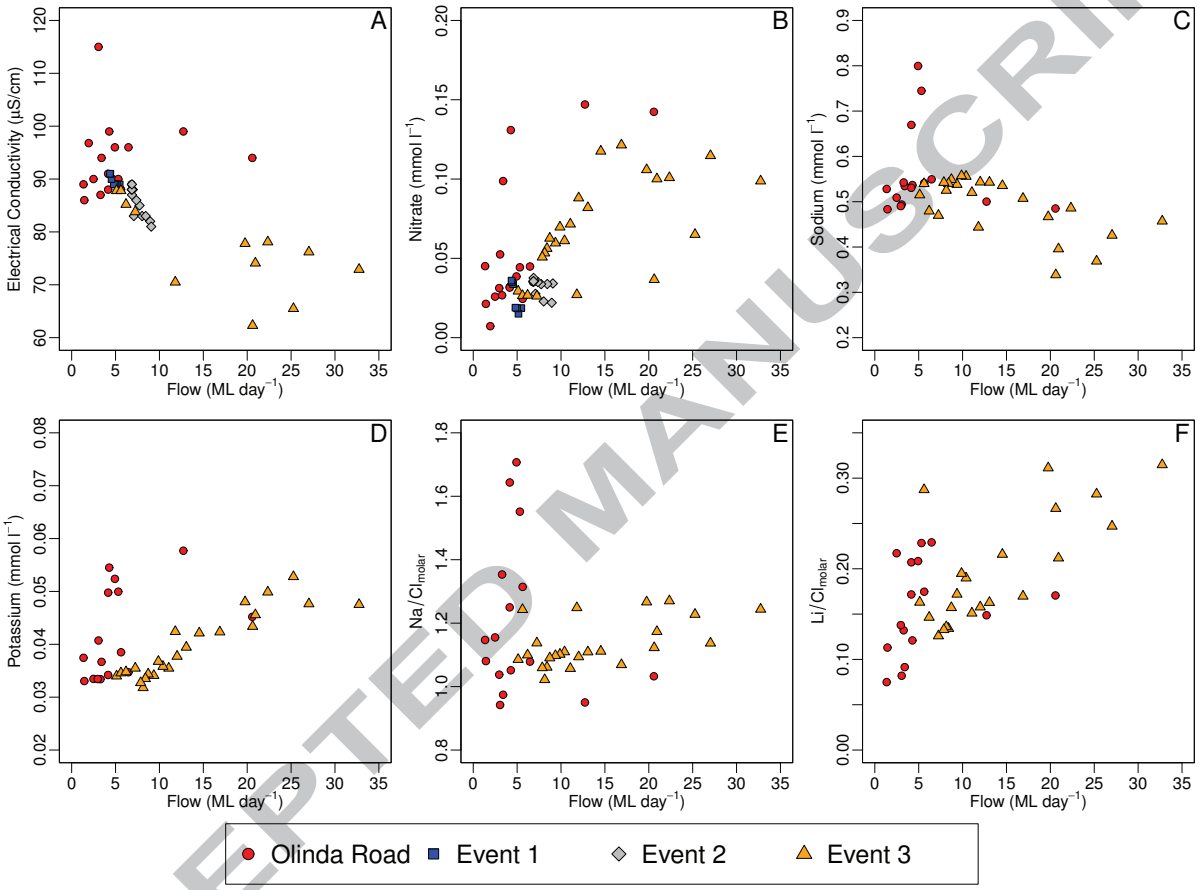

Figure 5: Plots of stream flow versus A) electrical conductivity, B) Nitrate, C) Sodium, D) Potassium, E) molar Na/Cl ratios and F) molar Li/Cl ratios for Lyrebird Creek at Olinda Road. Event 1, Event 2 and Event 3 represent the samples storm events mid October, end of October and November, respectively.

Table 2: Stable isotope, major ions, Lithium, ^{3}H and ^{222}Rn concentrations from Lyrebird Creek water at Olinda Road during the November 2013 storm event. *nm* = not measured.

Date/Time	δ^{18}O (‰VSMOW)	δ^{2}H (‰VSMOW)	F^- (mg L^{-1})	Cl^- (mg L^{-1})	Br^- (mg L^{-1})	NO_3^- (mg L^{-1})	$SO4^{2-}$ (mg L^{-1})	HCO_3- (mg L^{-1})	Na^+ (mg L^{-1})	K^+ (mg L^{-1})	Ca^2+ (mg L^{-1})	Mg^2+ (mg L^{-1})	Li^+ (mug L^{-1})	^{3}H (TU)	^{222}Rn (Bq m^{-3})
6/11/2013 12:00	-5.6	-31.9	0.03	14.21	0.07	1.66	2.1	9.6	12.47	1.306	1.399	1.69	0.367	1.559	784.72
12/11/2013 21:15	-5.8	-35.3	0.03	16.82	0.05	1.82	2.16	9.1	11.84	1.329	1.838	1.83	0.537	16.656	nm
13/11/2013 0:15	-6.1	-36.6	0.03	15.4	0.05	1.64	2.1	7.8	12.41	1.352	1.948	1.76	0.866	nm	nm
13/11/2013 3:15	-6.2	-36.4	0.04	15.46	0.05	1.66	2.16	7	11.02	1.36	1.459	1.671	0.443	nm	nm
13/11/2013 6:15	-6.7	-37.2	0.03	14.64	0.04	1.62	1.99	8	10.8	1.387	1.506	1.692	0.361	1.904	nm
13/11/2013 9:15	-7.1	-42.1	0.02	12.6	0.04	1.68	1.91	6	10.2	1.658	2.109	1.63	1.002	nm	nm
13/11/2013 12:15	-6.7	-39	0.03	10.69	0.01	2.27	1.91	5.3	7.785	1.696	1.314	1.191	0.558	2.274	nm
13/11/2013 15:00	-6.3	-36.6	0.04	10.65	0.03	4.03	2.07	2.8	8.479	2.064	1.247	1.204	0.589	2.411	nm
13/11/2013 18:15	-6.1	-35.2	0.03	11.96	0.03	6.21	2.17	4.8	9.1	1.782	1.254	1.317	0.496	2.491	nm
13/11/2013 21:15	-6	-34.6	0.03	13.06	0.04	6.56	2.22	5.6	10.73	1.878	1.462	1.503	0.796	2.409	nm
14/11/2013 0:15	-5.6	-33.2	0.03	13.56	0.04	6.25	2.13	4.8	11.17	1.95	3.042	1.782	1.339	nm	nm
14/11/2013 3:15	-6	-34.2	0.03	13.03	0.02	6.12	2.26	4.1	10.51	1.858	2.096	1.577	0.803	nm	nm
14/11/2013 6:15	-6.6	-33.6	0.03	13.28	0.03	7.11	2.4	3.8	9.79	1.863	1.625	1.659	0.642	nm	nm
14/11/2013 13:00	-5.9	-34	0.03	16.65	0.04	8.83	2.49	4.9	11.15	1.767	1.434	1.751	0.556	2.353	1357.22
14/11/2013 17:35	-5.7	-32.4	0.03	16.82	0.05	7.53	2.52	6.5	11.66	1.655	1.529	1.834	0.559	nm	nm
14/11/2013 23:35	-5.7	-31.9	0.02	17.08	0.05	7.29	2.08	6.3	12.31	1.647	1.816	1.98	0.722	nm	nm
15/11/2013 5:35	-5.6	-31.3	0.02	17.35	0.05	5.08	2.07	6.3	12.48	1.542	1.603	1.928	0.553	nm	nm
15/11/2013 11:35	-5.7	-32.5	0.03	17.61	0.05	5.46	2.02	6.5	12.49	1.475	1.49	1.895	0.544	nm	nm
15/11/2013 17:35	-5.7	-32.5	0.02	17.45	0.05	4.44	2.05	6.8	11.96	1.387	1.482	1.827	0.516	1.889	nm
15/11/2013 23:35	-5.7	-32.7	0.02	17.76	0.05	3.79	2.05	6.9	12.78	1.4	1.805	1.959	0.66	nm	nm
16/11/2013 5:35	-5.8	-32.7	0.03	17.93	0.05	4.32	2.01	7.3	12.81	1.437	1.607	1.904	0.684	nm	nm
16/11/2013 11:35	-5.7	-31.5	0.02	17.38	0.05	3.7	1.98	8	12.37	1.333	1.492	1.904	0.585	nm	nm
16/11/2013 17:35	-5.7	-32.4	0.03	17.85	0.05	3.89	2.01	8.2	12.62	1.344	1.405	1.828	0.549	nm	nm
16/11/2013 23:35	-5.7	-32.9	0.02	18.05	0.06	3.49	2.23	9.1	12.42	1.31	1.405	1.782	0.474	nm	nm
17/11/2013 5:35	-5.8	-31.1	0.03	18.22	0.06	3.31	2.22	7.8	12.07	1.243	1.355	1.723	0.485	nm	nm
17/11/2013 11:35	-5.7	-32.6	0.03	18.15	0.05	3.15	2.47	7.9	12.47	1.28	1.358	1.798	0.472	nm	nm
18/11/2013 14:00	-5.7	-31.4	0.03	18.06	0.06	2.78	2.22	8.5	12.63	1.357	1.317	1.703	0.81	1.802	1610.97

The ^{3}H activities of stream water at Olinda Road during the E3 event increased with increasing flow from 1.56 TU prior to the storm event at streamflows of 3.64 ML day^{-1} to a maximum of 2.49 TU at 20.92 ML day^{-1} streamflow close to the peak of the storm event. There was a similar increase in ^{3}H activities at Boundary Road from 1.7 TU prior to storm event E3 to 2.3 TU during the storm event. ^{3}H activities declined as streamflow fell but on November 18 (4 days after the peak) when streamflow was 6.8 ML day^{-1} the ^{3}H activity was still higher (1.8 TU) than those recorded before storm event E3. The interflow sample at Boundary Road collected during storm event E3 had a ^{3}H activity of 2.9 TU, which is higher than those recorded in the stream.

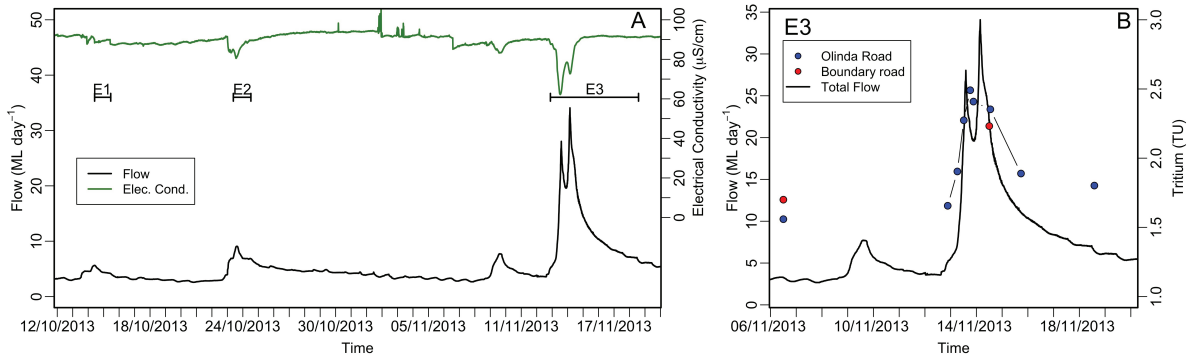

Figure 6: A) Three storm events were sampled in early October 2013 (E1), in late October 2013 (E2) and in mid-November 2013 (E3). Continuous electrical conductivity decreases during event 2 and 3 with increasing streamflow B) ^{3}H activities during the third event (E3) increase with increasing streamflow both at Olinda Road and at the top of the catchment at Boundary Road.

The δ^{18}O values of the monthly stream samples averaged -5.6 ‰ and Lyrebird Creek had similar δ^{18}O values at the start of each of the storm events. The first storm event E1 was not captured entirely and samples were only taken as streamflow receded (Fig. 7A). During the second storm event E2, δ^{18}O values of rainfall was -1.8 ‰, which was higher than the average δ^{18}O values of stream and groundwater δ^{18}O values. As a consequence, δ^{18}O values of the stream increased to -4.8 ‰ close to peak streamflows, decreased to -5.6 ‰ as the streamflows decreased. The δ^{18}O value of rainfall during storm event E3 was -10.63 ‰ and the δ^{18}O values of the stream water decreased with increasing flow. The minimum δ^{18}O value of -7.1 ‰ was reached on the 13th November at 9:15 approximately 5 hours before the first flow peak. The δ^{18}O values increased to ∼-5.6 ‰ and reached a second low of -6.6 ‰ at 6:15 on November 14 approximately 3 hours after the second peak (Tab. 2). δ^{18}O values subsequently increased to those close to the average δ^{18}O values in the stream water within a ∼3 hours and remained stable as streamflows decreased.

EC values were lower than the average of the stream water during each of the storm events and reached a minimum value of 62 μS/cm at the first peak of E3 (Fig. 6A). The EC increased between

the two flow peaks and reached a second minimum at the second flow peak. While the streamflow of this peak was higher than the first, the decrease in EC was less to 72 μS/cm; this is similar to the behaviour of the stable isotope data. Some of the major ion concentrations decreased during the peak streamflows while others increased. Na concentrations, for example, decreased during the peak streamflow of E3 but Na/Cl ratios remained nearly constant (Fig. 7 B and C). K concentrations and Li/Cl ratios increased from 1.2 to 1.3 mg L^{-1} and 0.1 to 0.16, to 2.06 mg L^{-1} and 0.50, respectively (Fig. 7D and F). NO_3 concentrations increased significantly with a peak of 9 mg L^{-1} at shortly after the second peak during E3 (Fig. 7E). Stream water ^{222}Rn activity was 784 Bq m^{-3} on the 6th November at low flows.

The ^{222}Rn activities of the stream water in the middle of the large storm event E3 on 14th November was 1 357 Bq m^{-3}. Water emerging from macropores of $\sim$1-2 cm in diameter had ^{222}Rn activities of 5 146 and 5 208 Bq m^{-3} on the same day. The macropores were approximately 50-100 cm underneath the surface and were accessible at the road cut of Boundary Road. The ^{222}Rn activity of one of these macropores that was still flowing a week later was 1 930 Bq m^{-3}.

4. Discussion

The small variation in major ion chemistry and stable isotopes at baseflow in the stream suggests that there is a single store of water generating the streamflow. Similar to catchments elsewhere in southeast Australia (Cartwright and Morgenstern, 2016), the Lyrebird Creek catchment is envisaged to be fed by a single store of water that becomes progressively older as the catchment receives less rainfall and dries up. Water originates then from deeper soils horizons and the saprolite. The greater variability in major ion chemistry and stable isotopes during the storm events suggest that discrete mixing between different water stores occurs at these times.

A two component hydrograph separation was used to separate between old and a young components of storm event streamflow at Olinda Road. We deliberately use the terms 'old' and 'young' and not 'ground water' and 'surface water' as we will show that surface water contributions are negligible and most of the runoff derives from subsurface stores. With rainwater Tritium activities of 3 TU (median of measured rain water activities) and old water activities of $\sim$1.56 TU in the week preceding the storm event the hydrograph separation reveals an overall old water contribution of $\sim$48 % (Fig. 8, Tab. 2). Similar results are achieved using EC and NO_3 with 45 % and 42 % old water component, respectively. EC values for old and new water were estimated from existing EC values for soil water (average of 154 μS/cm) and rain water (average of 30 μS/cm). NO_3 concentrations in shallow groundwater are lower than those in the soil water. During peak flow NO_3 increases to $\sim$9 mg L^{-1} indicating runoff generation from shallow soil and interception. The rainfall δ^{18}O value was

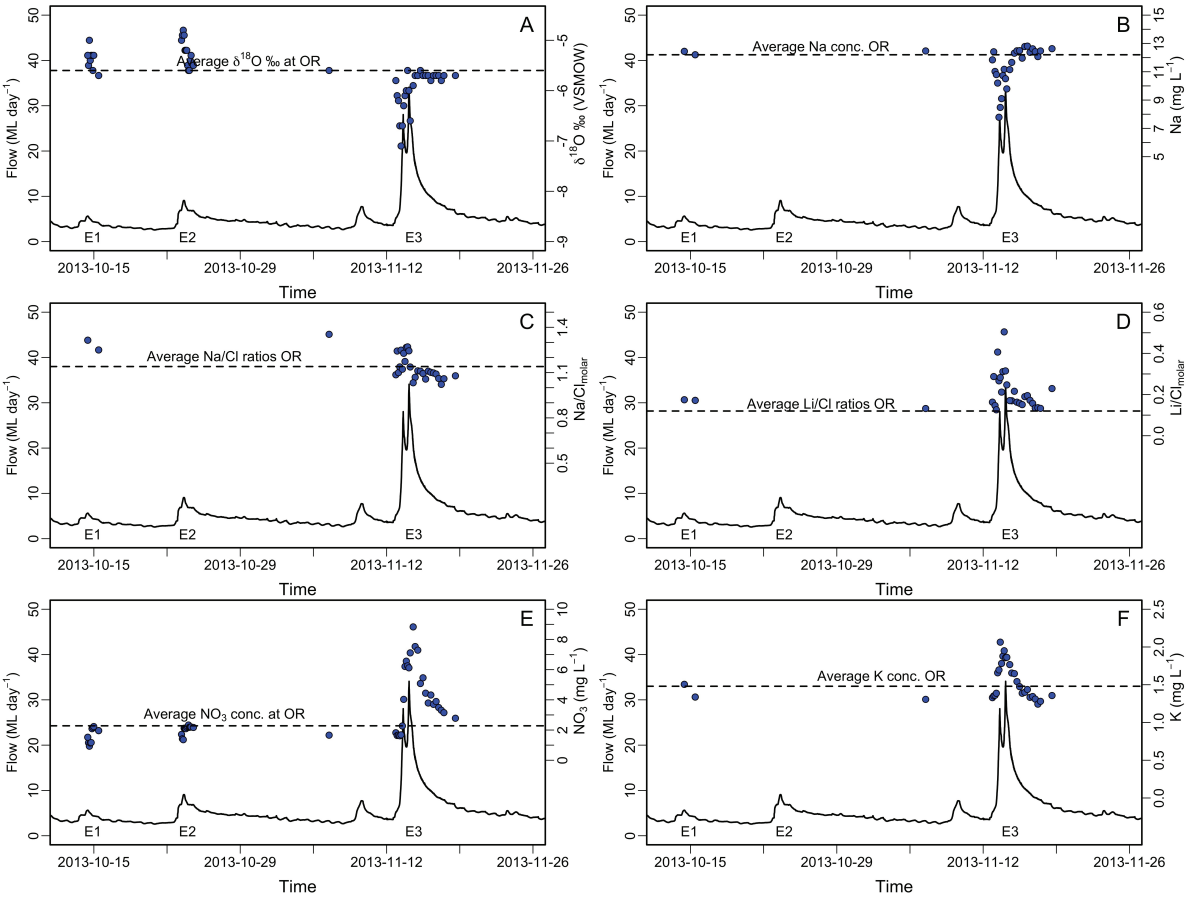

Figure 7: Plots show stream flow over time and changes of selected parameters. A) δ^{18}O, B) Na, C) Na/Cl, D) Li/Cl, E) NO_3 and F) K concentration of the stream water samples of Lyrebird Creek at Olinda Road during the three storm events in October and November 2013. The dashed lines represent the average values for δ^{18}O (A), Na (B), Na/Cl (C), Li/Cl (D), NO_3 (E) and K(F) in the stream water of Lyrebird Creek at Olinda Road.

-10.6 ‰ during E3. The old water δ^{18}O value is estimated as -5.5 ‰ $\pm$ 0.3 ‰ based on the average of baseflow, groundwater and soil water. The large difference between the rainwater δ^{18}O value of -10.6 ‰ and the δ^{18}O values of the streamflow during the storm event results in very high estimated old water contributions of 83 % (Fig. 8). The fact that the stable isotope values decrease towards rainfall values indicate that there is a change in water stores over the storm event with the majority of water from stores that do not have average δ^{18}O values. Furthermore, the observation that all three storm events have different shifts in δ^{18}O values implies that there is a component of inhomogenised water mixing with water from older stores discharging to the stream at these times (Fig. 7 A).

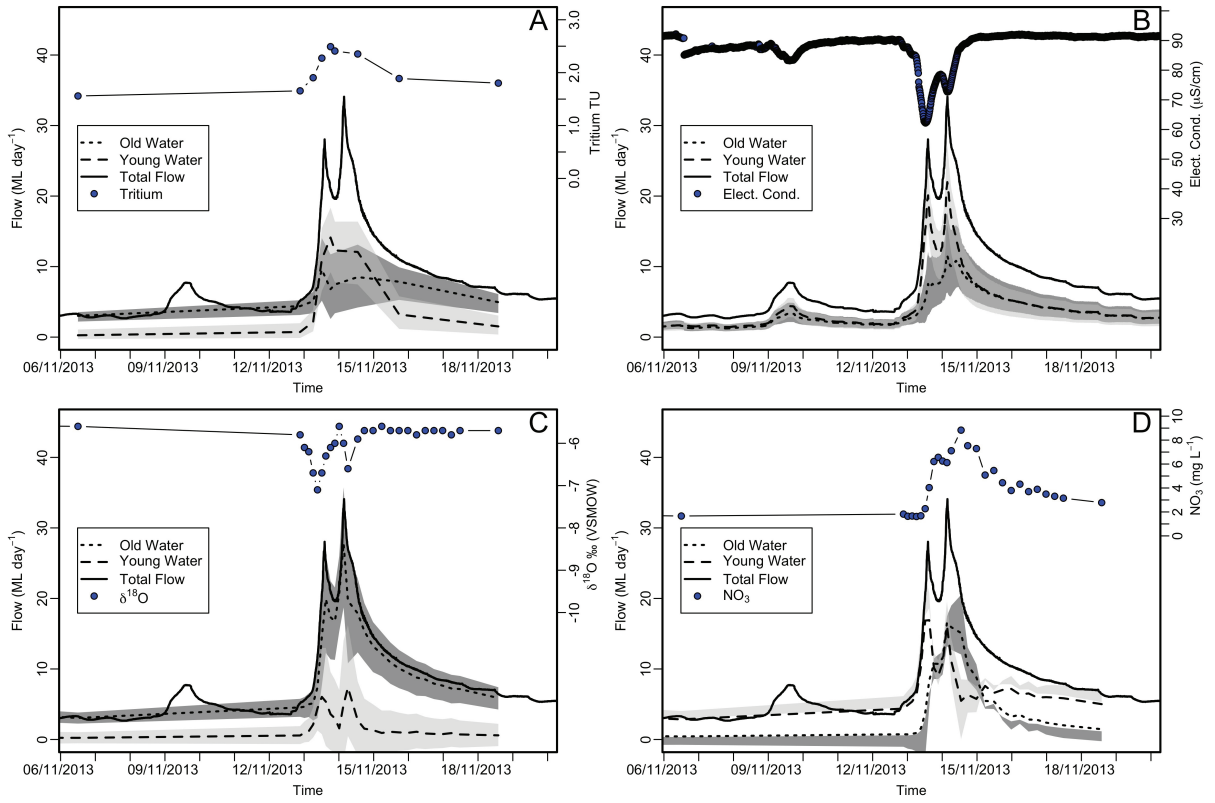

Figure 8: Plots of stream flow over time from early November 2013 to end November 2013 over the storm event E3. Blue points indicate the concentration of selected tracers, A) ^{3}H, B) electrical conductivity (EC) C) δ^{18}O, and D) NO_3. The dashed lines represent the proportions of old and young water of the total stream discharge derived from the hydrograph separation. Uncertainties are represented by the grey areas. Light grey for young water uncertainties and dark grey for old water uncertainties, respectively.

The mixing model indicates that the total flow during major storm events consists of at least half of old water sources of decadal time scales and a younger water from a source or sources, which is most likely in the range of multiple months to $<$ 5 years. The proportion of old water is $>$90 % during low flow periods and gets to a minimum of $\sim$50 % at high flow over entire storm events (^{3}H mass balance). The old water proportion is still 35 % at peak flow (Fig. 8) which was shown during the

storm event E3 in November 2013. Direct surface runoff only occurs to a small degree during very large storm events. In the absence of larger alluvial aquifers, all water stores must be located in the soil profile or saprolite. The flow age differences likely reflect which part of the soil profile is active. Younger water is likely stored in the upper parts of the soil while older water fills the deeper parts of the soils and the saprolite.

4.1. Mean transit times during baseflow

During baseflow streamflow is generated from a single store. Assuming that groundwater inflow from the deeper fractured rock aquifers is minimal most of the subsurface water will come from the soil and/or the saprolite/bedrock interface. In common with flow systems elsewhere in Australia, it is assumed that flow through the unsaturated zone follows a piston flow distribution, while the deeper soils, saprolite and fractured rock is characterised by exponential flow (Morgenstern et al., 2010; Stewart and Fahey, 2010; Duvert et al., 2016). Based on the studies by Morgenstern et al. (2010); Stewart and Fahey (2010); Duvert et al. (2016) that address flow in similar scale catchments, we calculated mean transit times using an exponential-piston flow model. A value for f of 0.85 successfully reproduced the time-series variation of tracers in some of those catchments and we initially adopt this value here (Fig. 9A; Tab. 1) (Morgenstern and Daughney, 2012). To assess the sensitivity of the transit time estimations to choice of model, mean transit times were also calculated using the exponential flow model (f=1) and the dispersion model (Fig. 9 B).

Melbourne has a long annual and sub-annual record of rainfall ^{3}H activities. The ^{3}H activity of rainfall in Melbourne peaked at $\sim$62 TU in 1965 and decreased exponentially to modern day rainfall weighted activities of between 2.8 and 3.2 TU by 1995 (International Atomic Energy Agency Global Network of Isotopes in Precipitation program, (Tadros et al., 2014)). The ^{3}H input function was based on the data of Tadros et al. (2014), which is derived from rainfall at Melbourne airport ($\sim$ 60 km from the study area), with missing values estimated by the function that describes the atmospheric ^{3}H activities for Melbourne. Based on the study of Tadros et al. (2014), the ^{3}H activity of modern rainfall collected at Monash University and the water samples from the discrete discharge points in the road cutting at Boundary Road during one of the major storm events, a ^{3}H activity of modern rainfall of 3 TU was utilised.

The estimated mean transit times differ between the models. The EPM produces generally younger estimates compared with the exponential model and the dispersion model (Fig. 9B). For the monthly samples, which represent the <Q10 flows, mean transit times estimated using the EPM vary from 43 years at the lowest streamflows (^{3}H=1.43 TU) to 33 years at higher streamflow (^{3}H=2.1 TU). These calculations used a ^{3}H activity of modern rainfall of 3 TU. The mean transit times of baseflow are

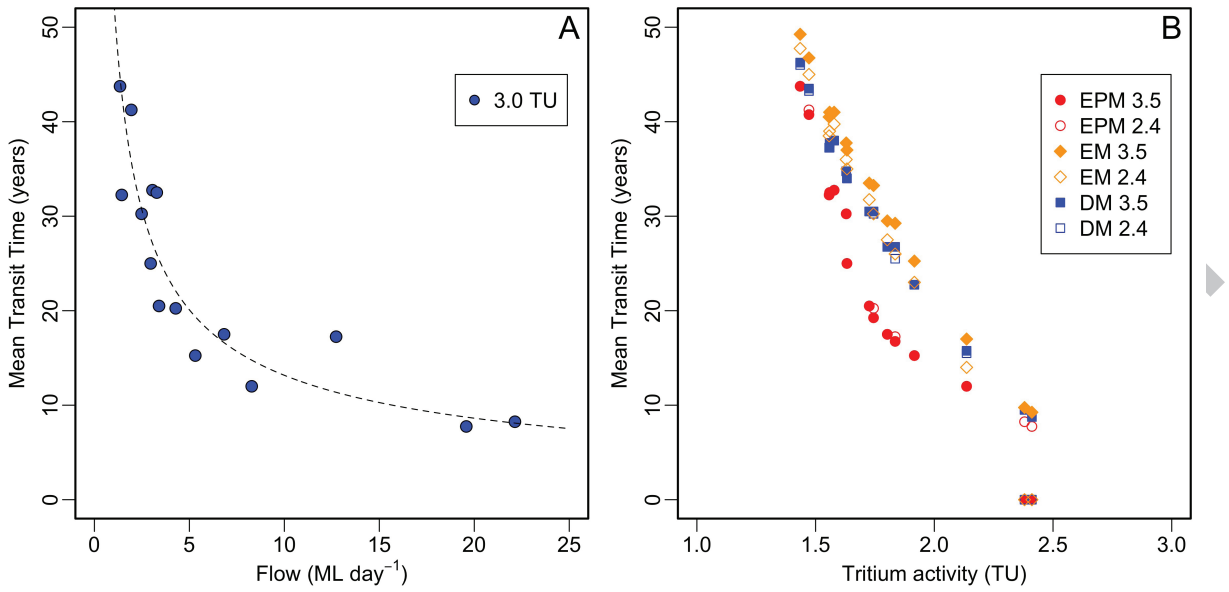

Figure 9: The figures shows the calculated mean transit times based on ^{3}H activities in the stream water in relation to flow. A) Change in mean transit times with flow for the samples from Olinda Road calculated using 3 TU (blue) as rainfall ^{3}H activity input value. B) Mean transit times calculated with the Exponential-Piston-Flow Model (EPM) (f=0.85), the Exponential Model (EM) and Dispersion Model (DM) for two rainfall input values, 2.4 TU and 3.5 TU.

relatively insensitive to the assumed ^{3}H activities of modern rainfall. For example, varying the ^{3}H activity of modern rainfall between 2.4 TU (highest value in stream water) and 3.5 TU (based on Tadros et al. (2014)) results in a range of mean transit times from the EPM of 0 to 46 years.

The decrease in mean transit times with increasing streamflow (Fig. 9A) suggests progressive activation of shallower, younger, water stores probably as the catchment 'wets up'. The mean transit times of the stream water during storm events is difficult to constrain with lumped parameter model as it is likely that there is discrete mixing between older and younger water stores in the catchment (this is discussed further below). However, the rapid decrease of ^{3}H activities in the stream after storm events suggests that most of the streamflow consists of several decades old water. Independent of the lumped parameter model approach taken or rainfall input function variability, ^{3}H activities lower than 1.8 TU imply mean transit times of $>$10 years, which is the upper limit of baseflow.

Monthly rainfall δ^{18}O records from the Global Network of Isotopes in Precipitation (GNIP) for Melbourne were analysed for a better understanding of long-term stable isotope fluctuations and seasonal trends. The long-term monthly average δ^{18}O indicate a clear seasonality for Melbourne with higher δ^{18}O values during summers and lower values during winter (Fig. 10). The δ^{18}O values of the stream water varied in a narrow range, with higher values in winter and lower values in summer (inverse to the rainfall trends). Transit times cannot be estimated from the stable isotopes but the

dampening of the rainfall stable isotope variations in the stream water implies that transit times are longer and that there is little direct input of rainfall or runoff.

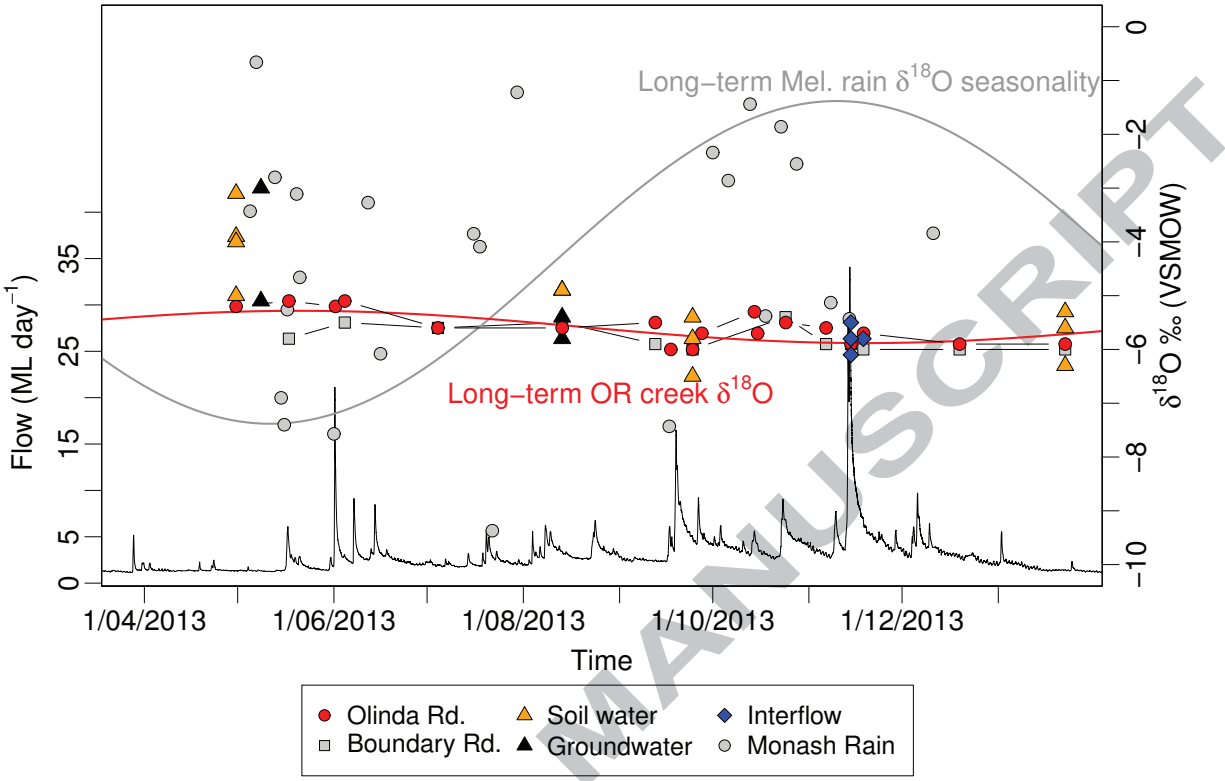

Figure 10: δ^{18}O and δ^{2}H values over the sampled years in relation to flow and rainfall variations. The grey curve indicates long-term (10year) seasonal variability of monthly stable isotope concentrations in rainfall (Global Network or Isotopes in Precipiation, 2016). The red line indicates the approximation of the variability in stable isotopes in the measured values from Lyrebird Creek at Olinda Road.

4.2. Source of water in the catchment

The water stores in the catchment most likely comprise soil water, groundwater from the fractured basement, and groundwater flowing along the boundary between the saprolite and the basement rocks. Groundwater flow through the fractured basement is probably a minor contributor to the overall streamflow of Lyrebird Creek and most streamflow is likely generated by water stored in the micro pores of the soil and saprolite. Macropore flow contributes significantly during storm events but ceases shortly after the rainfall has ceased.

The higher cation/Cl ratios in stream water, soilwater and shallow groundwater from the piezometers are compared to those of rainfall implies that mineral weathering occurs in the catchment. Na concentrations in the stream decrease during higher flows, Mg and Ca concentrations remain more

or less constant, while K concentrations and Li/Cl ratios increase (Fig. 3 A and B) indicating the weathered soil profile and the saprolite as main sources for the generated flow (Fig. 11).

Soils on the higher slopes have less undergrowth and have much lower organic matter content and the stream banks have finer sediments with much higher content of accumulated decomposing organic matter. Higher concentrations of NO_3 and K in the soil water are observed on the higher slopes of the catchment. These parts of the catchment then also get activated by the hydraulic loading during the storm events which increases NO_3 and K concentrations in the stream water (Goulding and Stevens, 1988; Thiffault et al., 2011; Oni et al., 2013). The fact that both NO_3 and K are relatively low during low flow (baseflow) indicates that the stores in the top soil are inactive at these times. At high flows low Na/Cl ratios and low tritium activities point towards a second subsurface water store. This water store is most likely in the saprolite which has most likely the longest flow paths from infiltration to discharge. Hence, an increase of solutes and older water ages are produced. In general, the large difference in hydraulic conductivity between bedrock and saprolite produces groundwater flow parallel to the slope along the boundary between the bedrock and the saprolite ((Brantley et al., 2011)).

The fact that the soils stores water during baseflow conditions and release water during storm events is also supported by the change in ^{222}Rn activities. While the use of ^{222}Rn is challenging as a quantitative tracer due to the difficulties in constraining degassing processes, it is an excellent tracer to detect subsurface discharge to a stream. The source of elevated ^{222}Rn activities in surface water is discharge of water from the sediments to the stream (Genereux and Hemond, 1990; Cartwright et al., 2014a).

Simultaneous increase of ^{222}Rn with higher streamflow at both sites suggests that most of the streamflow is generated from water displaced from the soils. This argument is further supported by ^{222}Rn activities in water from two macropores at Boundary Road during the major storm event in November 2013 which had ^{222}Rn activities that were much higher than those of the stream (5 146 and 5 208 Bqm^{-3}). One of the macropores was resampled a week later when flow had receded and had a ^{222}Rn activity of 1 930 Bq m^{-3}. The decrease in ^{222}Rn activities shortly after the main storm event suggests that preferential flow paths in the upper soils are activated during storm events and contribute the remaining part of the water to the total flow that is not coming from the deeper parts of the soil or from micropore flow. The water from the macropores at Boundary Road during E3 with the highest ^{222}Rn concentrations measured in the catchment and increasing K and NO_3 concentrations at Olinda road suggest that the infiltrating water must have mixed with the existing water in the catchment.

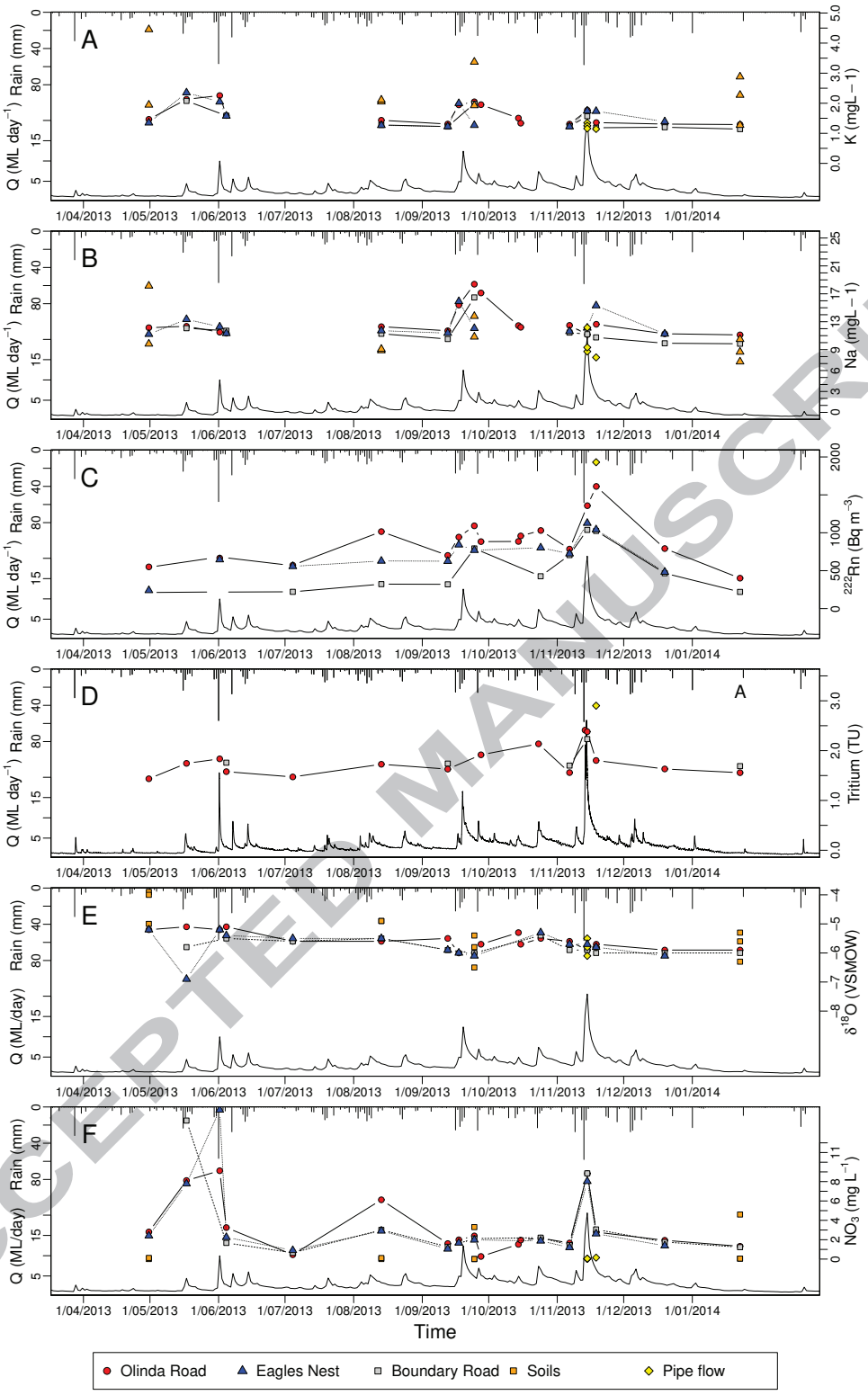

Figure 11: Chemical tracer concentrations during the sampled period from April 2013 to January 2014 with respect to rainfall (top of graphs) and streamflow (Q) (bottom of graphs). A) K concentrations with changing rainfall and streamflow, B) Na concentration with changing rainfall and streamflow, C) ^{222}Rn activities with changing rainfall and streamflow, D) ^{3}H activities with changing rainfall and streamflow, E) δ^{18}O ratios with changing rainfall and streamflow and F) NO_3 with changing rainfall and streamflow.

5. Conclusions and Implications

The use of ^{3}H time series in the Lyrebird catchment allowed a unique insight in the mean transit time distributions and flow system of this small temperate catchment in Victoria. The low ^{3}H activities at a range of streamflows and the fact that stream ^{3}H never reaches those of rainfall indicate that most of the flow in the stream derives from stores with long transit times. Calculated MTTs range from $\sim$6 to 40 years, which indicates the large retention potential for the catchment. This retention is most likely related to the micropore flow and flow through the saprolite at the soil-bedrock interface.

A slight discrimination along the flow paths is present. Most chemical parameter concentrations increase slightly from the headwater to the catchment outlet. The small increase however can be attributed to accumulation of major ions by mineral weathering (major cations, HCO_3) through longer flow paths through deeper soil layers.

There are three major stores in the catchment. The first is a deeper soil storage in the saprolite where water slowly flows to the stream. This causes the largest retention of the water due to longer flow paths as well as possibly lower hydraulic conductivities, which produce the oldest ages in the catchment. Simultaneously, weathering of the bedrock increases Na, K, Ca, Mg towards the lower parts of the catchment. The second and third stores are both located in the top soils and are possibly represented by a fast reacting store and one that has moderate transit times. A likely model for these two types of stores could be the difference in flow in micro and macro pores in the soil. Micro pores are the voids between mineral grains of the soil whereas macro pores are sub-surface channels resulting from either biological activity, such as root channels or worm holes, or geological forces, such as subsurface erosion , desciccation or synaeresis cracks and fractures. Micro pore flow is active once the catchment starts wetting up, increasing NO_3 and K concentrations as well as higher ^{222}Rn activities. Macro pore flow occurs during larger storm events. A significant increase in NO_3, K concentrations and ^{222}Rn activities at higher flows represents fast infiltrating rain water and a relatively rapid transfer towards the catchment's surface drainage systems. The high ^{3}H activities sample from the macro pore flow at Boundary Road during a storm event are consistent with the hypothesis that storm flow during very large storm events is very young water and must have infiltrated recently. The macro pore flow most likely mixes with some of the micro pore water along the flow paths in the top soil. Higher ^{222}Rn and NO_3 concentrations during the tail of the peak flows (November 2013) indicate that the micro pore flow can be active for several weeks until the catchment is restored baseflow conditions.

The results of this study have several implications. Mean transit times in headwater catchments are much longer than previously thought, in particular in a catchment that has high rainfall. Protec-

tion of headwater catchments is crucial for river flow further downstream as the water stores in the headwater are susceptible to land use changes. Deforestation might cause larger overland flow and less infiltration which subsequently influences long-term runoff from these catchments and the ability of catchments to buffer longer periods of little rainfall or droughts. More generally, this study illustrates the utility of ^{3}H for catchment studies, especially in the southern hemisphere and indicates that the traditional mean transit time estimations on flow data and stable isotope tracers underestimate the actual transit times by decades.

6. Acknowledgements

Funding for this project was provided by Monash University and the National Centre for Groundwater Research and Training. The National Centre for Groundwater Research and Training is an Australian Government initiative supported by the Australian Research Council and the National Water Commission via Special Research Initiative SR0800001. Parks Victoria granted access to work in the Dandenong National Park. We also would like to acknowledge Samantha Imberger, Mike Sammonds and Chris Walsh from the University of Melbourne who supplied the flow data for the catchment and Benjamin Gilfedder who assisted in the field.

7. References

Allaire, S. E., Roulier, S., Cessna, A. J., 2009. Quantifying preferential flow in soils: A review of different techniques. Journal of Hydrology 378 (1–2), 179 – 204.

Becker, A., 2005. Runoff Processes in Mountain Headwater Catchments: Recent Understanding and Research Challenges. Vol. 23 of Advances in Global Change Research. Springer Netherlands, Dordrecht, Ch. Runoff Processes in Mountain Headwater Catchments: Recent Understanding and Research Challenges, pp. 283–295.

Berne, A., Uijlenhoet, R., Troch, P. A., 2005. Similarity analysis of subsurface flow response of hillslopes with complex geometry. Water Resources Research 41 (9).

Beven, K., Germann, P., 2013. Macropores and water flow in soils revisited. Water Resources Research 49 (6), 3071–3092.

Blackburn, G., McLeod, S., 1983. Salinity of atmospheric precipitation in the Murray-Darling Drainage Division, Australia. Geochimica et Cosmochimica Acta 21, 411–434.

Bogaart, P. W., Rupp, D. E., Selker, J. S., van der Velde, Y., 2013. Late-time drainage from a sloping Boussinesq aquifer. Water Resources Research 49 (11), 7498–7507.

Brantley, S., Buss, H., Lebedeva, M., Fletcher, R., Ma, L., 2011. Investigating the complex interface where bedrock transforms to regolith. Applied Geochemistry 26, Supplement, S12 – S15, ninth International Symposium on the Geochemistry of the Earth's Surface (GES-9).

Burnett, W. C., Dulaiova, H., 2006. Radon as a tracer of submarine groundwater discharge into a boat basin in Donnalucata, Sicily. Continental Shelf Research 26 (7), 862–873.

Cartwright, I., Gilfedder, B., Hofmann, H., 2014a. Contrasts between estimates of baseflow help discern multiple sources of water contributing to rivers. Hydrology and Earth System Sciences 18 (1), 15–30.

Cartwright, I., Hofmann, H., 2016. Using radon to understand parafluvial flows and the changing locations of groundwater inflows in the Avon River, southeast Australia. Hydrology and Earth System Sciences 20 (9), 3581–3600.

Cartwright, I., Hofmann, H., Gilfedder, B., Smyth, B., 2014b. Understanding parafluvial exchange and degassing to better quantify groundwater inflows using ^{222}Rn: The King River, southeast Australia. Chemical Geology 380, 48–60.

Cartwright, I., Morgenstern, U., 2012. Constraining groundwater recharge and the rate of geochemical processes using tritium and major ion geochemistry: Ovens catchment, southeast Australia. Journal of Hydrology 475 (0), 137 – 149.

Cartwright, I., Morgenstern, U., 2015. Transit times from rainfall to baseflow in headwater catchments estimated using tritium: the Ovens River, Australia. Hydrology and Earth System Sciences 19 (9), 3771–3785.

Cartwright, I., Morgenstern, U., 2016. Using tritium to document the mean transit time and sources of water contributing to a chain-of-ponds river system: Implications for resource protection. Applied Geochemistry 75, 9 – 19.

Cartwright, I., Weaver, T. R., Cend/'on, D. I., Fifield, L. K., Tweed, S. O., Petrides, B., Swane, I., 2012. Constraining groundwater flow, residence times, inter-aquifer mixing, and aquifer properties using environmental isotopes in the southeast Murray Basin, Australia. Applied Geochemistry 17 (9), 1698–1709.

Cartwright, I., Weaver, T. R., Stone, D., Reid, M., 2007. Constraining modern and historical recharge from bore hydrographs, ^{3}H, ^{14}C, and chloride concentrations: Applications to dual-porosity aquifers in dryland salinity areas, Murray Basin, Australia. Journal of Hydrology 332, 69–92.

677 Cecil, L., Green, J., 2000. Radon-222. In: Cook, P., Herczeg, A. (Eds.), Environmental Tracers in
678 Subsurface Hydrogeology. Kluwer Academic Books, Boston, pp. 175–194.

679 Chabaux, F., Ma, L., Stille, P., Pelt, E., Granet, M., Lemarchand, D., di Chiara-Roupert, R., Brant-
680 ley, S. L., 2011. Determination of chemical weathering rates from u series nuclides in soils and
681 weathering profiles: Principles, applications and limitations. Applied Geochemistry 26, 20–23.

682 Clark, I. D., Fritz, P., 1997. Environmental Isotopes in Hydrogeology. Lewis Publischers.

683 Cook, P. G., 2013. Estimating groundwater discharge to rivers from river chemistry surveys. Hydro-
684 logical Processes 27 (35), 3694–3707.

685 Coplen, T., 1988. Normalization of oxygen and hydrogen isotope data. Chemical Geology 72 (293-
686 297).

687 Crouzet, E., Hubert, P., Olive, P., Siwertz, E., Marce, A., 1970. Le tritium dans les mesures
688 d'hydrologie de surface. determination experimentale du coefficient de ruissellement. Journal of
689 Hydrology 11 (3), 217 – 229.

690 Davies, J., Beven, K., Rodhe, A., Nyberg, L., Bishop, K., 2013. Integrated modeling of flow and res-
691 idence times at the catchment scale with multiple interacting pathways. Water Resources Research
692 49 (8), 4738–4750.

693 Duvert, C., Stewart, M. K., Cendón, D. I., Raiber, M., 2016. Time series of tritium, stable isotopes
694 and chloride reveal short-term variations in groundwater contribution to a stream. Hydrology and
695 Earth System Sciences 20 (1), 257–277.

696 Edmunds, W. M., 2009. Geochemistry's vital contribution to solving water resource problems. Ap-
697 plied Geochemistry 24 (6), 1058–1073.

698 Freeman, M. C., Pringle, C. M., Jackson, C. R., 2007. Hydrologic connectivitz and the contribu-
699 tion of stream headwates to ecological integrity at regional scales. Journal of the American Water
700 Resources Association 43 (1), 5–14.

701 Fritz, S. J., Drimmie, R. J., Fritz, P., 1991. Characterizing shallow aquifers using tritium and ^{14}C:
702 periodic sampling based on Tritium half-life. Applied Geochemistry 6 (1), 17 – 33.

703 Gaillardet, J., Dupré, B., Louvat, P., Allègre, C., 1999. Global silicate weathering and CO_2 consump-
704 tion rates deduced from the chemistry of large rivers. Chemical Geology 159 (1–4), 3 – 30.

Genereux, D., Hemond, H., 1990. Naturally occuring Radon-222 as a tracer for streamflow generation: steady-state methodology and field example. Water Resources Research 26 (12), 3065–3075.

Global Network or Isotopes in Precipiation, I., 2016.

Godsey, S. E., Kirchner, J. W., Clow, D. W., 2009. Concentration-discharge relationship reflect chemostatic characteristics of US catchments. Hydrological Processes 23, 1844–1864.

Goulding, K., Stevens, P., 1988. Potassium reserves in a forested, acid upland soil and the effect on them of clear-felling versus whole-tree harvesting. Soil Use and Management 4 (2), 45–51.

Gusyev, M. A., Toews, M., Morgenstern, U., Stewart, M., White, P., Daughney, C., Hadfield, J., 2013. Calibration of a transient transport model to tritium data in streams and simulation of groundwater ages in the western lake taupo catchment, new zealand. Hydrology and Earth System Sciences 17 (3), 1217–1227.

Herczeg, A. L., Edmunds, W. M., 2000. Inorganic ions as tracers. In: Cook, P. G., Herczeg, A. L. (Eds.), Environmental Tracers in Subsurface Hydrogeology. Kluwer Academic Publishers, p. 529.

Hofmann, H., Cartwright, I., 2013. Using hydrogeochemistry to understand inter-aquifer mixing in the on-shore part of the Gippsland Basin, southeast Australia. Applied Geochemistry 33 (0), 84 – 103.

Hrachowitz, M., Savenije, H., Bogaard, T. A., Tetzlaff, D., Soulsby, C., 2013. What can flux tracking teach us about water age distribution patterns and their temporal dynamics? Hydrology and Earth System Sciences 17 (2), 533–564.

Hugenschmidt, C., Ingwersen, J., Sangchan, W., Sukvanachaikul, Y., Duffner, A., Uhlenbrook, S., Streck, T., 2014. A three-component hydrograph separation based on geochemical tracers in a tropical mountainous headwater catchment in northern Thailand. Hydrology and Earth System Sciences 18 (2), 525–537.

Jencso, K. G., McGlynn, B. L., 11 2011. Hierarchical controls on runoff generation: Topographically driven hydrologic connectivity, geology, and vegetation. Water Resources Research 47 (11).

Jurgens, B. C., Böhlke, J., Eberts, S. M., 2012. Tracerlpm (version 1): An excel® workbook for interpreting groundwater age distributions from environmental tracer data. Tech. rep., US Geological Survey Water Resources Investigations.

Kennedy, V., Kendall, C., Zellweger, G., Wyerman, T., Avanzino, R., 1986. Determination of the components of stormflow using water chemistry and environmental isotopes, Mattole River Basin, California. Journal of Hydrology 84 (1), 107 – 140.

Kienzler, P. M., Naef, F., 2008. Subsurface strom flow formation at different hillslopes and implications for the 'old water paradox'. Hydrological Processes 22, 104–116.

Kirchner, J. W., 2003. A double paradox in catchment hydrology and geochemistry. Hydrological Processes 17, 871–874.

Kirchner, J. W., Tetzlaff, D., Soulsby, C., 2010. Comparing chloride and water isotopes as hydrological tracers in two Scottish catchments. Hydrological Processes 24, 1631–1645.

Klaus, J., Chun, K. P., McGuire, K. J., McDonnell, J. J., 2015. Temporal dynamics of catchment transit times from stable isotope data. Water Resources Research 51 (6), 4208–4223.

Klaus, J., Zehe, E., Elsner, M., Külls, C., McDonnell, J. J., 2013. Macropore flow of old water revisited: Experimental insights from a tile-drained hillslope. Hydrology and Earth System Sciences 17 (1), 103–118.

Kumar, A., Kanwar, R., Hallberg, G., 1997. Separating preferential and matrix flows using subsurface tile flow data. Journal of Environmental Science and Health . Part A: Environmental Science and Engineering and Toxicology 32 (6), 1711–1729.

Lamontagne, S., Cook, P., 2007. Estimation of hyporheic water residence time in situ using ^{222}Rn disequilibrium. Limnology and Oceanography: Methods 5, 407–416.

Leaney, F., Smettem, K., Chittleborough, D., 1993. Estimating the contribution of preferential flow to subsurface runoff from a hillslope using deuterium and chloride. Journal of Hydrology 147 (1), 83 – 103.

Maloszewski, P., 2000. Lumped-parameter models as a tool for determining the hydrological parameters of some groundwater systems based on isotope data. In: Tracer and Modelling in Hydrogeology - Proceetings of the TraM'2000 Conference. IAHS Publ. no. 262, Liege, Belgium, pp. 271–276.

Maloszewski, P., Rauert, W., Stichler, W., Herrmann, A., 1983. Application of flow models in an alpine catchment area using tritium and deuterium data. Journal of Hydrology 66 (1-4), 319–330.

Maloszewski, P., Rauert, W., Trimborn, P., Herrmann, A., Rau, R., 1992. Isotope hydrological study of mean transit times in an alpine basin (Wimbachtal, Germany). Journal of Hydrology 140 (1–4), 343 – 360.

763 Maloszewski, P., Zuber, A., 1982. Determining the turnover time of groundwater systems with the aid
764 of environmental tracers. Journal of Hydrology 57, 207–231.

765 McCallum, J. L., Cook, P. G., Brunner, P., Berhane, D., 2010. Solute dynamics during bank storage
766 flows and implications for chemical base flow separation. Water Resources Research 46.

767 McDonnell, J., Bonell, M., Stewart, M., Pearce, A., 1990. Deuterium variations in storm rainfall:
768 Implications for stream hydrograph separation. Water Resources Research 26 (3), 455–458.

769 McDonnell, J., McGuire, K., Aggarwal, P., Beven, K., Biondi, D., Destouni, G., Dunn, S., James, A.,
770 Kirchner, J., Kraft, P., Lyon, S., Maloszewski, P., Newman, B., Pfister, L., Rinaldo, A., Rodhe, A.,
771 Sayama, T., Seibert, J., Solomon, K., Soulsby, C., Stewart, M., Tetzlaff, D., Tobin, C., Troch, P.,
772 Weiler, M., Western, A., Wörman, A., Wrede, S., 2010. How old is streamwater? Open questions
773 in catchment transit time conceptualization, modelling and analysis. Hydrological Processes 24,
774 1745–1754.

775 McGuire, K. J., McDonnell, J. J., 2006. A review and evaluation of catchment transit time modeling.
776 Journal of Hydrology 330, 543–563.

777 Morgenstern, U., Daughney, C. J., 2012. Groundwater age for identification of baseline groundwater
778 quality and impacts of land-use intensification - The National Groundwater Monitoring Programme
779 of New Zealand. Journal of Hydrology 456–457 (0), 79 – 93.

780 Morgenstern, U., Daughney, C. J., Leonard, G., Gordon, D., Donath, F. M., Reeves, R., 2015. Using
781 groundwater age and hydrochemistry to understand sources and dynamics of nutrient contamina-
782 tion through the catchment into lake rotorua, new zealand. Hydrology and Earth System Sciences
783 19 (2), 803–822.

784 Morgenstern, U., Stewart, M., Stenger, R., 2010. Dating of streamwater using tritium in a post nuclear
785 bomb pulse world: Continuous variation of mean transit time with streamflow. Hydrology and Earth
786 System Sciences 14, 2289–2301.

787 Morgenstern, U., Taylor, C. B., 2009. Ultra low-level tritium measurement using electrolytic enrich-
788 ment and lsc. Isotopes in Environmental and Health Studies 45 (2), 96–117, pMID: 20183224.

789 Oni, S. K., Futter, M. N., Bishop, K., Köhler, S. J., Ottosson-Löfvenius, M., Laudon, H., 2013. Long-
790 term patterns in dissolved organic carbon, major elements and trace metals in boreal headwater
791 catchments: Trends, mechanisms and heterogeneity. Biogeosciences 10 (4), 2315–2330.

Rice, K., Hornberger, G. M., 1998. Comparison of hydrochemical tracers to estimate source contributions to peak flow in a small, forested, headwater catchment. Water Resources Research 34 (7), 1755–1766.

Rodgers, P., Soulsby, C., Waldron, S., 2005. Stable isotope tracers as diagnostic tools in upscaling flow path understanding and residence time estimates in a mountainous mesoscale catchment. Hydrological Processes 19 (11), 2291–2307.

Sklash, M., Farvolden, R., 1979. The role of groundwater in storm runoff. Journal of Hydrology 43, 45–65.

Sophocleous, M., 2002. Interactions between groundwater and surface water: The state of the science. Hydrogeology Journal 10, 52–67.

Soulsby, C., Tetzlaff, D., 2008. Towards simple approaches for mean residence time estimation in ungauged basins using tracers and soil distributions. Journal of Hydrology 363 (1–4), 60 – 74.

Stewart, M., Fahey, B., 2010. Runoff generating processes in adjacent tussock grassland and pine plantation catchments as indicated by mean transit time estimation using tritium. Hydrology and Earth System Sciences 14, 1021–1032.

Stewart, M. K., Morgenstern, U., McDonnell, J. J., 2010. Truncation of stream residence time: How the use of stable isotopes has skewed our concept of streamwater age and origin. Hydrological Processes 24, 1646–1659.

Stumpp, C., Maloszewski, P., 2010. Quantification of preferential flow and flow heterogeneities in an unsaturated soil planted with different crops using the environmental isotope δ^{18}O. Journal of Hydrology 394 (3–4), 407 – 415.

Surbeck, H., 1993. Radon monitoring in soils and water. Nuclear Tracks and Radiation Measurement 22 (1-4), 463–468.

Tadros, C. V., Hughes, C. E., Crawford, J., Hollins, S. E., Chisari, R., 2014. Tritium in Australian precipitation: a 50 year record. Journal of Hydrology 513, 262–273.

Tekleab, S., Wenninger, J., Uhlenbrook, S., 2014. Characterisation of stable isotopes to identify residence times and runoff components in two meso-scale catchments in the Abay/Upper Blue Nile Basin, Ethiopia. Hydrology and Earth System Sciences 18 (6), 2415–2431.

820 Tetzlaff, D., Soulsby, C., Waldron, S., Malcolm, I. A., Bacon, P. J., Dunn, S. M., Lilly, A., Youngson,
821 A. F., 2007. Conceptualization of runoff processes using a geographical information system and
822 tracers in a nested mesoscale catchment. Hydrological Processes 21 (10), 1289–1307.

823 Thiffault, E., Hannam, K. D., Paré, D., Titus, B. D., Hazlett, P. W., Maynard, D. G., Brais, S., 2011.
824 Effects of forest biomass harvesting on soil productivity in boreal and temperate forests — a review.
825 Environmental Reviews 19, 278–309.

826 Timbe, E., Windhorst, D., Celleri, R., Timbe, L., Crespo, P., Frede, H.-G., Feyen, J., Breuer, L.,
827 2015. Sampling frequency trade-offs in the assessment of mean transit times of tropical montane
828 catchment waters under semi-steady-state conditions. Hydrology and Earth System Sciences 19 (3),
829 1153–1168.

830 Tweed, S. O., Weaver, T. R., Cartwright, I., 2005. Distinguishing groundwater flow paths in different
831 fractured-rock aquifers using groundwater chemistry: Dandenong Ranges, Southeast Australia.
832 Hydrogeology Journal 13, 771–786.

833 Tweed, S. O., Weaver, T. R., Cartwright, I., Schaefer, B., 2006. Behavior of rare earth elements in
834 groundwater during flow and mixing in fractured rock aquifers: An example from the Dandenong
835 Ranges, Southeast Australia. Chemical Geology 234, 291–307.

836 van Schaik, N. L. M. B., Bronstert, A., de Jong, S. M., Jetten, V. G., van Dam, J. C., Ritsema, C. J.,
837 Schnabel, S., 2014. Process-based modelling of a headwater catchment in a semi-arid area: The
838 influence of macropore flow. Hydrological Processes 28 (24), 5805–5816, hYP-11-0613.

839 Vogel, T., Sanda, M., Dusek, J., Dohnal, M., Votrubova, J., 2010. Using oxygen-18 to study the role
840 of preferential flow in the formation of hillslope runoff. Vadose Zone Journal 9, 252–259.

841 Zuber, A., Witczak, S., Rózański, K., Śliwka, I., Opaka, M., Mochalski, P., Kuc, T., Karlikowska,
842 J., Kania, J., Jackowicz-Korczyński, M., Duliński, M., 2005. Groundwater dating with ^{3}H and SF_6
843 in relation to mixing patterns, transport modelling and hydrochemistry. Hydrological Processes
844 19 (11), 2247–2275.

845

- Tritium time series to establish baseflow mean transit times in headwater catchment.
- Chemical hydrograph separation using stream tritium data
- Tritium in stream never reaches rainfall Tritium input values